Global and Planetary Change 137 (2016) 131–148

Contents lists available at ScienceDirect

Global and Planetary Change

journal homepage: www.elsevier.com/locate/gloplacha

Invited review article

Lake oxygen isotopes as recorders of North American Rocky Mountain hydroclimate: Holocene patterns and variability at multi-decadal to millennial time scales

Lesleigh Anderson [a,*], Max Berkelhammer [b], John A. Barron [c], Byron A. Steinman [d], Bruce P. Finney [e], Mark B. Abbott [f]

[a] U.S. Geological Survey Geosciences and Environmental Change Science Center, Denver, CO, USA
[b] University of Illinois-Chicago, Department of Earth and Environmental Science, Chicago, IL, USA
[c] U.S. Geological Survey Volcano Science Center, Menlo Park, CA, USA
[d] University of Minnesota-Duluth, Department of Earth and Environmental Sciences and Large Lakes Observatory, Duluth, MN, USA
[e] Idaho State University, Departments of Biological Sciences and Geosciences, Pocatello, ID, USA
[f] University of Pittsburgh, Department of Geology and Environmental Science, Pittsburgh, PA, USA

ARTICLE INFO

Article history:
Received 31 July 2015
Received in revised form 6 December 2015
Accepted 29 December 2015
Available online 2 January 2016

Keywords:
Lake water isotopes
Holocene
Western North America
Paleoclimate
Ocean–atmosphere
Climate forcing

ABSTRACT

Lake sediment oxygen isotope records (calcium carbonate-$\delta^{18}O$) in the western North American Cordillera developed during the past decade provide substantial evidence of Pacific ocean–atmosphere forcing of hydroclimatic variability during the Holocene. Here we present an overview of 18 lake sediment $\delta^{18}O$ records along with a new compilation of lake water $\delta^{18}O$ and $\delta^{2}H$ that are used to characterize lake sediment sensitivity to precipitation-$\delta^{18}O$ in contrast to fractionation by evaporation. Of the 18 records, 14 have substantial sensitivity to evaporation. Two records reflect precipitation-$\delta^{18}O$ since the middle Holocene, Jellybean and Bison Lakes, and are geographically positioned in the northern and southern regions of the study area. Their comparative analysis indicates a sequence of time-varying north–south precipitation-$\delta^{18}O$ patterns that is evidence for a highly non-stationary influence by Pacific ocean–atmosphere processes on the hydroclimate of western North America. These observations are discussed within the context of previous research on North Pacific precipitation-$\delta^{18}O$ based on empirical and modeling methods. The Jellybean and Bison Lake records indicate that a prominent precipitation-$\delta^{18}O$ dipole (enriched-north and depleted-south) was sustained between ~3.5 and 1.5 ka, which contrasts with earlier Holocene patterns, and appears to indicate the onset of a dominant tropical control on North Pacific ocean–atmosphere dynamics. This remains the state of the system today. Higher frequency reversals of the north–south precipitation-$\delta^{18}O$ dipole between ~2.5 and 1.5 ka, and during the Medieval Climate Anomaly and the Little Ice Age, also suggest more varieties of Pacific ocean–atmosphere modes than a single Pacific Decadal Oscillation (PDO) type analogue. Results indicate that further investigation of precipitation-$\delta^{18}O$ patterns on short (observational) and long (Holocene) time scales is needed to improve our understanding of the processes that drive regional precipitation-$\delta^{18}O$ responses to Pacific ocean–atmosphere variability, which in turn, will lead to a better understanding of internal Pacific ocean–atmosphere variability and its response to external climate forcing mechanisms.

Published by Elsevier B.V.

Contents

* Corresponding author.
E-mail address: land@usgs.gov (L. Anderson).

http://dx.doi.org/10.1016/j.gloplacha.2015.12.021
0921-8181/Published by Elsevier B.V.

1. Introduction

North American Rocky Mountain winter precipitation, principally stored as snowpack, is the primary water resource for the surrounding semiarid regions (Wise, 2012). North American precipitation patterns and corresponding snowpack distributions reflect synoptic scale winter storm tracks and the upper level atmospheric flow (Changnon et al., 1993; L'Heureux et al., 2004; Shinker and Bartlein, 2009; Miyasaka et al., 2014). Significant snowpack variance is explained by ocean–atmosphere climate modes, which are internal to the climate system and operate on interannual to multi-decadal times-scales, such as the El Niño Southern Oscillation (ENSO) and the Pacific Decadal Oscillation (PDO) (Dettinger et al., 1998; Cayan et al., 1998; Brown and Comrie, 2004; Mote, 2006; Brown, 2011; Pederson et al., 2011). Changing atmospheric flow provides a potential mechanistic explanation for correlations between precipitation distributions (both spatial and temporal) and internal climate modes such as ENSO and PDO.

The role and significance of internal ocean–atmosphere climate variability, and its responses to external forcing mechanisms, such as changes in Earth's orbital configuration, volcanism, and anthropogenic activity, are prominently featured in questions about the future of water resources in western North America (Pederson et al., 2013; McCabe and Wolock, 2009; Wise, 2010; Byrne et al., 1999; Clark et al., 2001; Salathé, 2006; Hoerling et al., 2010; Abatzoglou, 2011). However, application of multi-decadal climate mode concepts is complex because such atmospheric behavior emerges in the climate system even in the absence of external forcing and thereby comprises background climate variability, or noise, which is inherently stochastic (Alexander, 2010; Schneider and Cornuelle, 2005; Overland et al., 2008).

Estimates of future responses of western North American water resources to anthropogenic warming are provided by General Circulation Models (GCMs) (Barnett and Pierce, 2009; Seager et al., 2007). GCMs accurately capture many aspects of the climate system, including the global response to external forcing, which provide important insight into the dynamics associated with past and future climate change. However, many GCMs consistently appear to either suppress or inaccurately represent internal ocean–atmosphere variability and should not be exclusively relied upon to investigate future climate change scenarios for regions that are strongly influenced by internal climate modes such as western North America (Alder and Hostetler, 2014; Bartlein et al., 2014; Collins, 2005; Deser et al., 2012; Harrison et al., 2014, 2015; Schmidt et al., 2005; Sun, 2010).

Holocene climate proxy records provide abundant evidence for changes in internal ocean–atmosphere climate variability related to external forcing (e.g., Cobb et al., 2013; Koutavas and Joanides, 2012; Li et al., 2011; Moy et al., 2002). Here we review evidence that internal ocean–atmosphere climate variability affects hydroclimate in western North America in response to external forcing from spatially distributed lake isotope records (carbonate-$\delta^{18}O$) with an emphasis on the records that reflect the oxygen isotope composition of precipitation (precipitation-$\delta^{18}O$). Such records provide insight on past changes in atmospheric flow, moisture source areas, rainout efficiency, and the temperature of condensation (Ingraham, 1998; Darling et al., 2006). We propose that with a process-based understanding of regional climate controls on precipitation-$\delta^{18}O$, inferred precipitation patterns and corresponding atmospheric flow from spatially distributed precipitation-$\delta^{18}O$ paleorecords will elucidate the changing influence of North Pacific ocean–atmosphere variability on Rocky Mountain snowpack on multi-decadal to millennial time scales.

To achieve our objectives, we evaluate 18 lake carbonate-$\delta^{18}O$ records within the greater western North American Cordillera from Alaska to Colorado (Fig. 1). Our evaluation is based on a compilation of lake water isotope values ($\delta^{18}O$ and $\delta^{2}H$) that provide a framework for understanding the $\delta^{18}O$ relationships between lake-sediment carbonate (endogenic calcite and aragonite), lake water, and precipitation. This allows us to characterize each of the lake carbonate-$\delta^{18}O$ records as an "isometer" of the climate processes that control precipitation, precipitation minus evaporation (P − E), or a mixture of both. We then use the Holocene precipitation-$\delta^{18}O$ records to examine north–south precipitation-$\delta^{18}O$ patterns on multi-decadal to millennial timescales. From this comparative analysis we consider how internal Pacific ocean–atmosphere modes varied throughout the Holocene and influenced hydroclimate in the western North American Cordillera in relation to external forcing by solar insolation. This comparison necessitates a review of previous research on precipitation-$\delta^{18}O$ in the North Pacific and Gulf of Alaska region.

2. Lake water-$\delta^{18}O$ and carbonate-$\delta^{18}O$

We focus this analysis on the interior Rocky Mountain region where there are strong continental rainout fractionation effects on precipitation-$\delta^{18}O$ (Winnick et al., 2014). The lake carbonate-$\delta^{18}O$ records are distributed from northern Alaska (~68°N) to southern Colorado (~37°N), and we also include a discussion of the Mount Logan ice-$\delta^{18}O$ record in the Yukon Territory (Fisher et al., 2004, 2008), the Oregon Caves National Monument (NM) speleothem-$\delta^{18}O$ record (Ersek et al., 2012), and the Gulf of Alaska (GoA) foraminiferal-$\delta^{18}O$ record EW0408-85JC (Praetorius and Mix, 2014) (Fig. 1a, Table 1). Additional lake and speleothem carbonate-$\delta^{18}O$ records from the desert environments of the Great Basin (Benson et al., 2002, 2003; Lachniet et al., 2014; Yuan et al., 2004, 2013), and the Sierra Nevada in California (McCabe-Glyn et al., 2013) are not included in the present analysis, which we have limited to intermountain regions with higher precipitation amounts.

The intermountain lake records span a range of climates indicated by the ratio of precipitation (P) to potential evaporation (PE) derived from the National Centers for Environmental Prediction North American Regional Reanalysis (NCEP-NARR). The NARR is a three-dimensional atmospheric model forced with observed climate from surface measurements and atmospheric soundings (Mesinger et al., 2006). The model is fundamentally similar to global reanalysis products but is projected onto a 0.3° × 0.3° horizontal grid that makes it particularly useful for studies of topographically complex environments. The large-scale P/PE patterns (Fig. 1a) reflect topographic effects on the amount of precipitation where regions with the highest ratios, indicative of a wetter climate, occur in low elevation coastal areas and particularly along the coastal mountain ranges, largely due to higher P. Lower P/PE ratios, which indicate a drier climate, occur in leeward rain shadows of mountain ranges: these are found in eastern Washington, the southwest Yukon Territory, and low elevation regions of Colorado and Utah, due to low P and high PE. Intermediate ratios typically reflect areas with highly uneven seasonal precipitation distributions where the amount

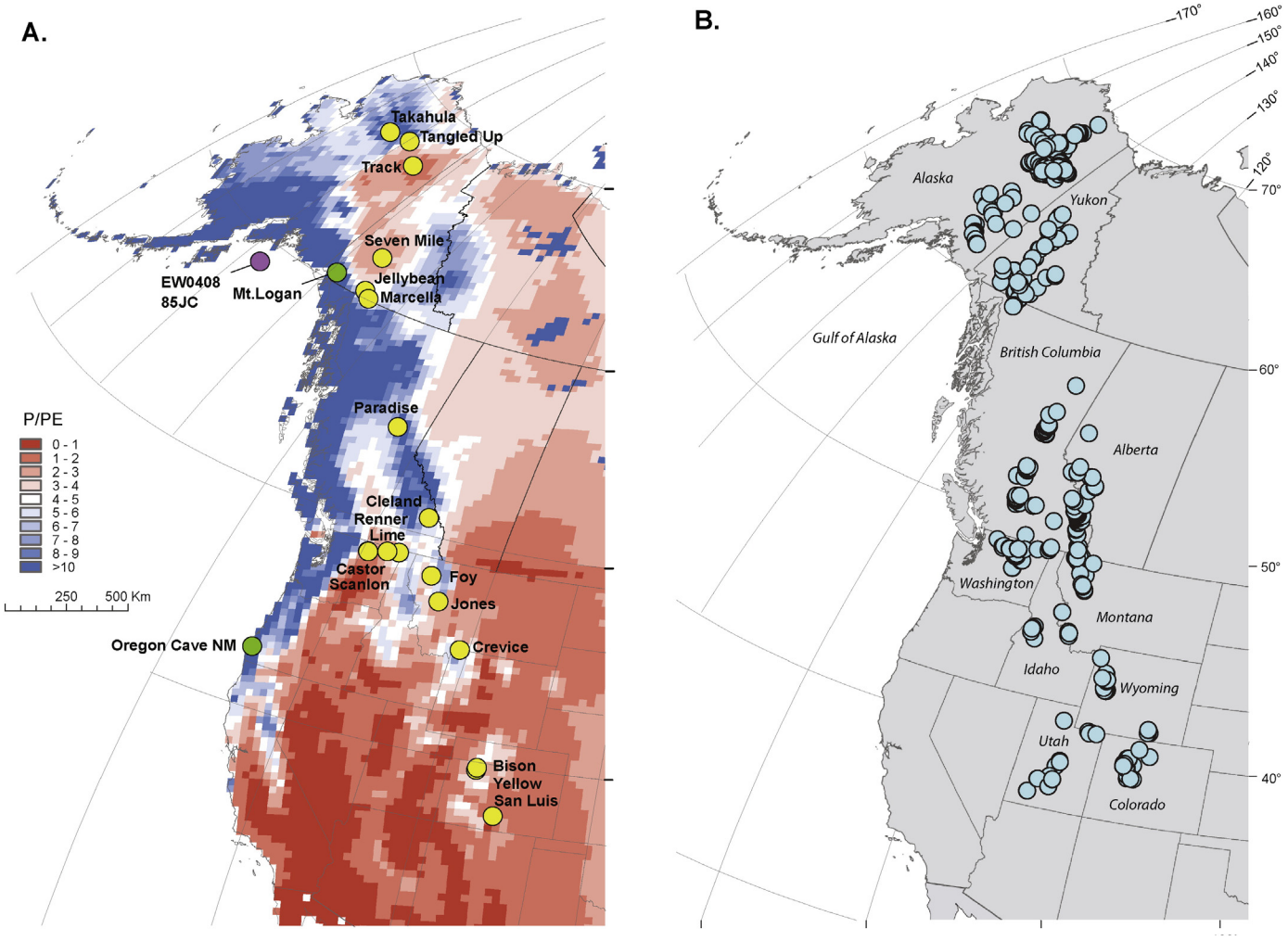

Fig. 1. Western North American (A) gridded NCEP-NARR precipitation/potential evaporation ratios (P/PE, scaled values for visualization) and locations of lake sediment-$\delta^{18}O$ records (yellow; Table 1), and $\delta^{18}O$ records from Gulf of Alaska (GoA) planktonic foraminifera EW0408-85JC (purple), Mount Logan ice core (green), and Oregon Cave NM speleothem (green). (B) Locations of compiled lake water $\delta^{18}O$ and $\delta^{2}H$ compositions (Table 2, Supplementary files).

Table 1
Lake carbonate-$\delta^{18}O$ records.

Name	Lat (°N)	Long (°W)	Elev (m)	ka[a]	P/PE[b]	P (kg/m^2)	PE (kg/m^2)	*dxs*	Isometer	Reference
Takahula	67.35	153.66	257	11	8.03	1.17	0.15	−4.7	Mixed	Clegg and Hu (2010)
Tangled Up	67.67	149.715	416	7	7.14	1.20	0.17	−1.6	Precipitation	Anderson et al. (2001)
Track	66.85	145.169	145	5	1.69	0.50	0.29	−41.4	Mixed	Anderson, this study
Seven Mile	62.18	136.38	503	1	2.67	0.71	0.27	−37.3	Mixed	Anderson et al. (2011)
Jellybean	60.35	134.80	727	8	4.82	1.13	0.24	7.0	Precipitation	Anderson et al. (2005)
Marcella	60.073	133.806	454	5	4.79	1.16	0.24	−42.0	P/E	Anderson et al. (2007)
Paradise	54.684	122.616	733	10	10.04	2.76	0.28	−5.7	Mixed	Steinman et al. (2014)
Cleland	50.832	116.39	1158	10	6.07	1.66	0.28	−42	P/E	Steinman, this study
Castor	48.541	119.581	604	6	1.99	0.91	0.46	−45.5	P/E	Nelson et al. (2011)
Scanlon	48.54	119.56	702	0.1	1.99	0.91	0.46	−43.8	P/E	Steinman et al. (2013)
Lime	48.873	117.338	781	10	5.29	2.35	0.45	7.6	Precipitation	Steinman et al. (2012)
Renner	48.78	118.189	757	1.5	2.99	1.48	0.50	−1.2	Mixed	Steinman, this study
Foy	48.163	114.353	1010	2.2	3.81	1.64	0.43	−32.7	P/E	Stevens et al. (2006)
Jones	47.04	113.142	1250	12.5	3.28	1.48	0.45	−20	Mixed	Shapley et al. (2009)
Crevice	45.00	110.578	1709	10	5.14	2.38	0.46	*	Mixed	Whitlock et al. (2013)
Bison	39.765	107.345	3290	10	3.47	1.67	0.48	10.5	Precipitation	Anderson (2011)
Yellow	39.651	107.345	3160	7	3.47	1.67	0.48	−2.7	Mixed	Anderson (2012)
San Luis	37.67	105.72	2290	11	1.91	1.07	0.56	*	Mixed	Yuan et al. (2013)

[a] Time length of record, thousands of years.
[b] North American Regional Reanalysis (NARR), precipitation = P and potential evaporation = PE.
* Modern water data not available.

of P is high but dominated by winter snowfall and PE is also high during relatively long dry summers, such as in the northern and central Rocky Mountains in Montana and Colorado.

Based on the compilation of ~600 lake water $\delta^{18}O$ and $\delta^{2}H$ measurements (Fig. 1b), similar climate controls are also evident from regional evaporation lines (REL) derived from lake water isotope compositions and their intercept with the Global Meteoric Water Line (GMWL) (Fig. 2a). The compilation includes previously published data as well as newly presented results (Supplemental files). We identified eight regional groups from the water isotope data and determined the linear

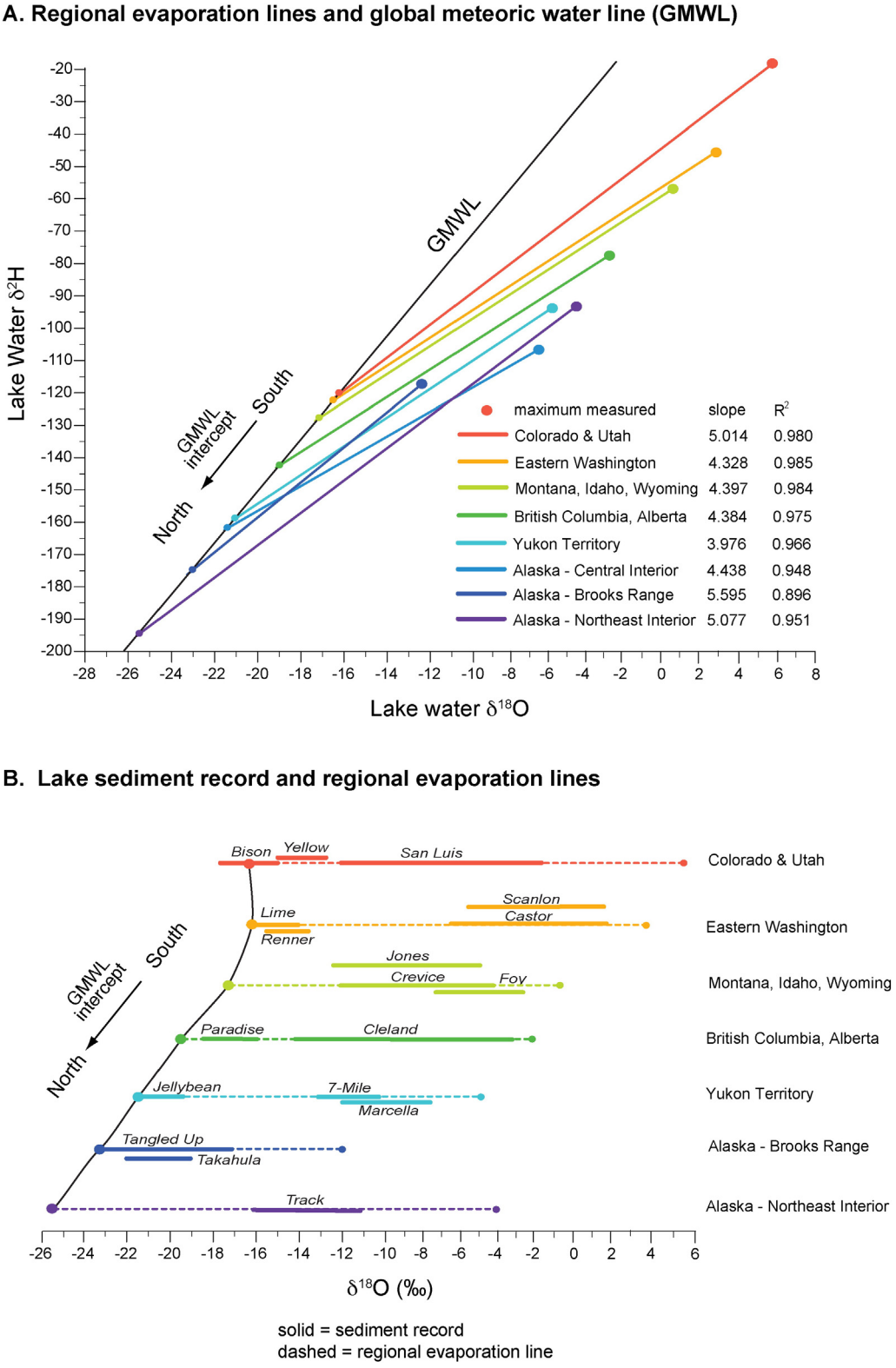

Fig. 2. (A) Regional Evaporation Lines for eight western North American regions (REL; colored vectors) derived from lake water $\delta^{18}O$ and $\delta^{2}H$ compositions (n ~ 600; Table 2 and supplementary files) and the Global Meteoric Water Line (GMWL; black vector). Solid circles indicate the maximum isotopic compositions observed for each region. (B) Lake carbonate-$\delta^{18}O$ records (solid) on their respective REL (dashed) and generalized $\delta^{18}O$ scale (same color and order as in A).

Table 2
Western North America Regional Evaporation Line (REL) statistics.

Region	n	R^2	REL-GMWL Intercept $\delta^{18}O$	Slope	Reference[a]
Brooks Range Alaska	68	0.8959	−23.27	5.595	Clegg and Hu (2010), Finney (this study)
Northeast Interior Alaska	99	0.9513	−25.61	5.077	Anderson et al. (2013)
Central Interior Alaska	33	0.9475	−21.19	4.438	Finney and Anderson (this study)
Yukon Territory	69	0.9659	−21.55	3.976	Anderson et al. (2005, 2007)
British Columbia & Alberta	114	0.9758	−19.52	4.384	Steinman and Abbott (this study)
Eastern Washington	115[b]	0.9846	−16.62	4.328	Steinman et al. (2012, this study)
Montana, Idaho, & Wyoming	82	0.9844	−17.33	4.397	Henderson and Shuman (2009), Steinman and Abbott (this study)
Colorado & Utah	100	0.9804	−16.43	5.014	Anderson (2011, 2012, this study)

[a] Regional plots and all data are available in Supplemental files.
[b] Includes 75 measurements of Castor and Scanlon Lakes.

$\delta^{18}O$ and $\delta^{2}H$ correlations, REL, for each (Table 2): Colorado and Utah, Montana, Wyoming and Idaho, eastern Washington, British Columbia and Alberta, Yukon Territory, and within Alaska, the central interior, southern Brooks Range, and northeast interior. The intercept of each REL with the GMWL indicates the starting isotopic composition of the regional source waters on an evaporation-driven vector, and therefore, closely approximates the annual weighted $\delta^{18}O$ value of precipitation (Darling et al., 2006).

The decline in $\delta^{18}O$ value for the REL-GMWL intercept for higher latitudes reflects large-scale climatic controls on regional precipitation-$\delta^{18}O$, including latitude and continental effects (Bowen and Wilkinson, 2002; Kendall and Coplen, 2001; Rozanski et al., 1993). The $\delta^{18}O$ intercept values of −25.5‰ in northeast interior Alaska at ~65°N represent a −9.5‰ difference in $\delta^{18}O$ value for the REL-GMWL intercept in Colorado and Utah at ~40°N. The more positively enriched intercept values in Colorado and Utah (−16‰ and −118‰ for $\delta^{18}O$ and $\delta^{2}H$, respectively) are due to the region's low latitude, warmer temperatures, and frequent incursions of subtropical Pacific and Gulf of Mexico air masses, which bring relatively enriched $\delta^{18}O$ and $\delta^{2}H$ vapor to the region. At higher latitudes, more negatively depleted intercepts are due to colder temperatures and the dominance of North Pacific and Arctic vapor relatively depleted in $\delta^{18}O$ and $\delta^{2}H$. The seasonal balance of precipitation is also influential such that snow-dominated climates are characterized by depleted intercepts.

A broadly similar spatial precipitation-$\delta^{18}O$ pattern for this region is also evident from the Global Network of Isotopes in Precipitation (GNIP; Bowen and Wilkinson, 2002; Rozanski et al., 1993). However, it is crucial to recognize the isotopic differences between lake water and precipitation estimates because it is the isotope ratio of lake water, rather than precipitation, that is incorporated by the lake sediment carbonate-$\delta^{18}O$ proxy, which is our focus here. The substantial differences amongst the RELs also make it evident that assessments of individual lake water isotope data should be based on each lake's comparison with its respective regional evaporation trends.

The REL slopes range from ~4.0 (Yukon Territory) to 5.6 (southern Brooks Range in Alaska), and reflect the influence of relative humidity on kinetic fractionation (Gibson et al., 2016; Henderson and Shuman, 2009). Lower slopes indicate relatively high evaporation and low relative humidity (low P/PE) and they are observed for all the sampled regions from Colorado to the Yukon Territory and central Alaska (slopes of 3.9 to 4.4). Higher slopes in northern Alaska (5.0 and 5.5) reflect a combination of higher precipitation and humidity and a limitation on total evaporation imposed by the short ice-free warm season.

REL length, represented here as the range of lake isotope values observed in each region, is strongly associated with the distribution of the sampling and individual basin hydrology (Steinman and Abbott, 2013; Supplemental files) but is also likely influenced by P/PE. For instance, higher maximum isotope compositions and longer REL length are observed for regions with lower relative humidity and longer warm seasons during which evaporation strongly influences lake water isotopic composition. Thus, isotope values from Colorado and Utah have the longest REL and the shortest REL in the southern Brooks Range in Alaska reflects that region's high P/PE and the combined effects of higher relative humidity and short ice-free warm season.

The position of an individual lake's isotopic composition relative to its REL indicates the extent to which fractionation resulting from evaporation enriches the remaining water in heavy isotopes relative to the original isotopic composition of meteoric source water, which is the inflow and direct precipitation on the lake's surface. Thus, the distance between an individual lake's isotopic composition and the value of the REL-GMWL intercept is a function of the extent to which evaporation has influenced a lake's water-$\delta^{18}O$. From this observation of modern lake water-$\delta^{18}O$ we take the approach that past lake sensitivity to evaporation can also be generally evaluated by the position of sediment carbonate-$\delta^{18}O$ values on their respective modern REL (Fig. 2b). The greater the distance between the range of carbonate-$\delta^{18}O$ values and REL-GMWL intercept likely indicates an increasing control by evaporation on lake water-$\delta^{18}O$ throughout a lake's history.

For a visual comparison of the 18 carbonate-$\delta^{18}O$ records along each REL we use a generalized horizontal $\delta^{18}O$ scale (Fig. 2b). This representation again highlights the decline in REL-GMWL intercepts from $\delta^{18}O$ values of −17 to −18‰ in southern latitudes (upper) to −20 to −25.5‰ in higher latitudes (lower). Several carbonate-$\delta^{18}O$ records, such as Scanlon, Castor, Foy, Cleland and Marcella Lakes, are nearer the maximum lake water-$\delta^{18}O$ value within a region. Others span the middle of their RELs, such as San Luis, Jones, Crevice, 7-Mile and Track Lakes. Several carbonate-$\delta^{18}O$ records are nearer to their REL-GMWL intercept value, such as Yellow, Renner, Paradise, and Takahula Lakes, whereas Bison, Lime, Jellybean, and Tangled Up Lakes overlap their REL-GMWL intercept.

Since $\delta^{18}O$ measurements are reported as per mil deviations (‰) in relation to two different standards, the international Vienna-Pee-Dee Belemnite standard (VPDB) for carbonate and Standard Mean Ocean Water (VSMOW) for water, and there is a lake water-temperature fractionation effect between carbonate minerals and water (~ 0.25‰/°C; Friedman and O'Neil, 1977), adjustments are needed in order to compare water and carbonate $\delta^{18}O$. However, these differences are relatively small in comparison to the range of the carbonate-$\delta^{18}O$ values for each record and do not significantly alter these general comparisons.

As previous reviews of oxygen isotopes from lake sediments have summarized (Ito, 2001; Leng et al., 2006; Leng and Marshall, 2004), understanding the sensitivity of lake water to evaporation-driven fractionation effects is critical for correctly assessing the paleoclimate information provided by lake carbonate-$\delta^{18}O$ variations. Along these lines, our evaluation further elucidates the reasons why comparison of lake carbonate-$\delta^{18}O$ variations must account for differences in the climate sensitivity of each lake system resulting from regional climate and extent of hydrological closure. If these considerations are ignored, the resulting interpretations can be misleading and lead to spurious reconstructions of past climate conditions. Our evaluation here is based on identifying the relationship of a particular lake's water isotope values to the appropriate REL-GMWL intercept, thus providing a framework for carbonate-$\delta^{18}O$ paleoclimate studies in northwestern North America.

2.1. Lakes as "isometers"

As a reservoir of meteoric water, a lake's isotopic composition is a metric of the controlling climate and hydrologic processes and can be considered an "isometer." The hydrologic fluxes of water into and out of a lake control the degree to which lake water-$\delta^{18}O$ reflects changes in precipitation-$\delta^{18}O$, P − E, or both (Fig. 3). On one end of the hydrologic spectrum are hydrologically open lakes with water residence times that are too short for evaporation to significantly influence the water body. In this case, high rates of surface and subsurface inflow and outflow lead to water residence times of days to weeks for small lake systems. Although evaporation does influence the lake, its effects on the isotope mass balance of the overall water body are minimal due to continual replacement by runoff and groundwater inflow. This hydrologic configuration often leads to lake water-$\delta^{18}O$ values that reflect precipitation-$\delta^{18}O$, and we term these systems "precipitation isometers." They are identified by water isotope values that plot on the intersection of the REL and the GMWL, or with the regional meteoric water line if it has been established. As discussed above, there are four lakes in western North America that appear to fit this criteria; Bison Lake in Colorado, Lime Lake in eastern Washington, Jellybean Lake in the southwest Yukon Territory, and Tangled Up Lake in the Brooks Range of northern Alaska (Fig. 2b).

On the other end of the hydrologic spectrum are lakes in which outflow is restricted and significant water loss occurs through evaporation from the lake surface. In such terminal lake systems, climate changes may drive both lake level and lake water-$\delta^{18}O$ variations; if inflow exceeds evaporation for a long period of time, then lake levels rise and lake water-$\delta^{18}O$ decreases, and vice-versa, leading to transient isotopic shifts to hydrologic forcing rather than long-term isotope equilibrium responses to hydroclimate (Gat, 1995; Ricketts and Anderson, 1998; Steinman and Abbott, 2013; Shapley et al., 2008). A large number of lakes fall between the fully open and fully closed end members and have some surface and subsurface outflow, typically as subsurface

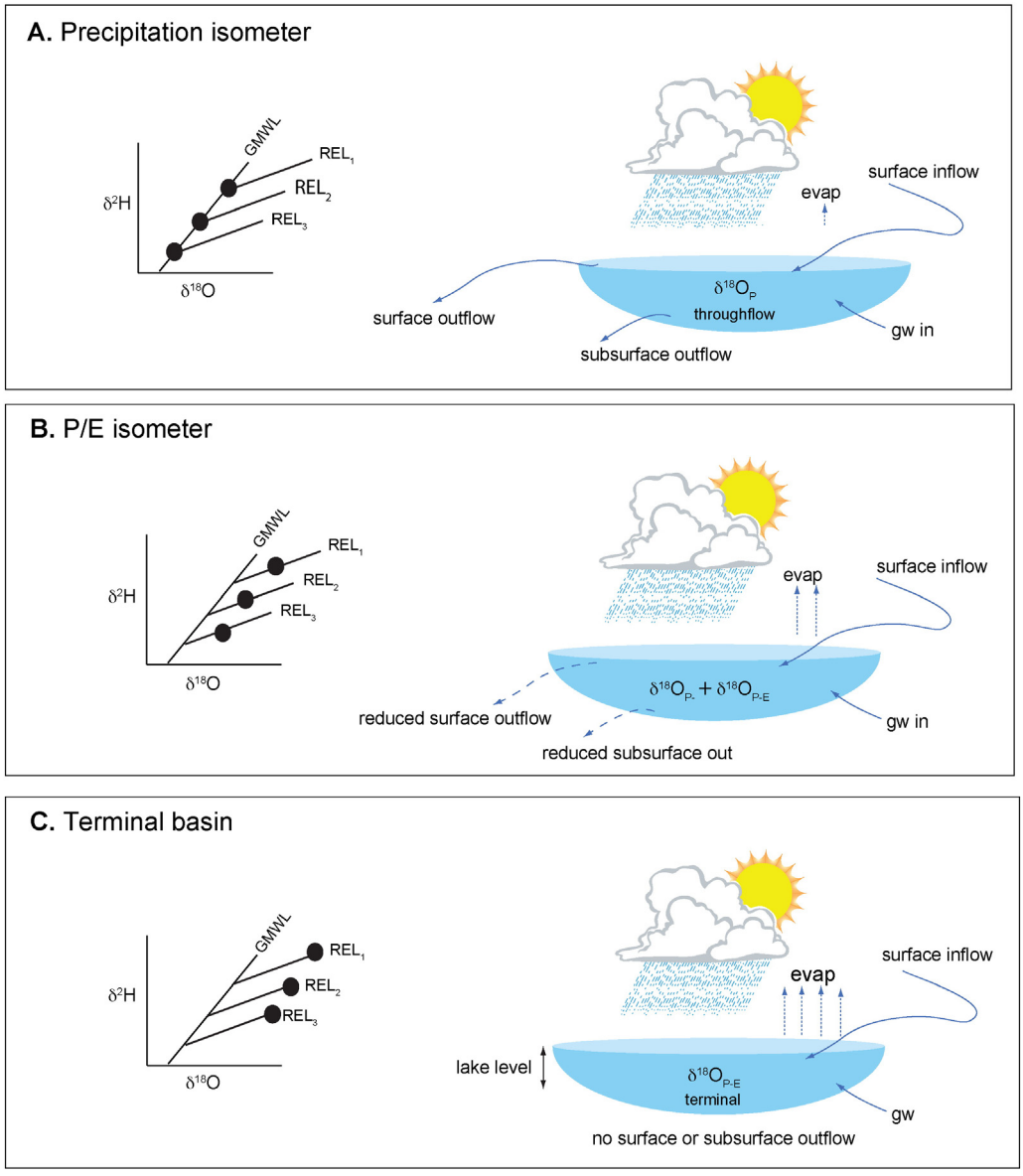

Fig. 3. Schematic of lake hydrology showing the influence on lake-$\delta^{18}O$ by the relative strength of evaporative loss to input; (A) in open, through-flowing systems, lake-$\delta^{18}O$ is minimally fractionated by evaporation and reflects precipitation-$\delta^{18}O$, (B) in P − E systems lake-$\delta^{18}O$ reflects precipitation-$\delta^{18}O$ and fractionation by evaporation, and (C) in fully closed, terminal systems, all water loss is by evaporation and lake $\delta^{18}O$ is strongly enriched. Schematic plots of $\delta^{18}O$ and $\delta^{2}H$ (as in Fig. 2a) for each example indicates the relative positions of lake-$\delta^{18}O$ (black circles) on three hypothetical regional evaporation lines (REL_1, REL_2, REL_3) extending from the Global Meteoric Water Line (GMWL). ($\delta^{18}O_P$ = precipitation-$\delta^{18}O$, $\delta^{18}O_{P-E}$ = evaporated lake water-$\delta^{18}O$, gw = groundwater, evap = evaporation flux).

seepage through the littoral zones, but restriction may also occur if surface outflow is regulated by a fixed outflow elevation and is therefore intermittent. These systems, that we term here as "P — E isometers," also lose substantial amounts of water through evaporation from the lake surface.

For P — E isometer hydrologic configurations, which characterize the majority of the 18 lake systems discussed here, site-specific hydrologic controls on lake water residence time and evaporation are best evaluated on a case-by-case basis with isotope mass balance modeling tools (Gibson et al., 2016; Shapley et al., 2008, Anderson et al. 2011). Because these systems indicate transient and equilibrium lake water-$\delta^{18}O$ responses to hydroclimate change, the carbonate-$\delta^{18}O$ records reflect both short-term (sub-decadal to decadal) and long-term (centennial to millennial) forcing (Steinman and Abbott, 2013; Steinman et al., 2010, 2012). Five P — E lake records approach the maximum lake water-$\delta^{18}O$ on their RELs, which indicates significant fractionation by evaporation: Castor and Scanlon Lakes in eastern Washington, Foy Lake in Montana, Cleland Lake in British Columbia, and Marcella Lake in Yukon Territory. The remaining nine lake records, at intermediate positions between GMWL intercepts and water-$\delta^{18}O$ maxima, indicate more balanced controls by both precipitation-$\delta^{18}O$ and evaporation (Fig. 2b, identified as "mixed" in Table 2).

Many of these records were evaluated as part of a prior study that focused on western North American lake carbonate P — E isometers with an emphasis on identifying climate shifts during the past 2000 years (Steinman et al., 2014). Most of these records (Marcella, Paradise, Cleland, Renner, Castor, Foy, Jones, and Crevice) have sufficient temporal resolution to identify recent multi-decadal to century scale variability and their geographic distribution is sufficient to characterize regional patterns.

The general relationships between lake water-$\delta^{18}O$, hydrology, and climate are also indicated by the ~600 lake water deuterium excess values (*dxs*) shown with the NARR P/PE ratios (Fig. 4). The *dxs* is calculated from $\delta^{18}O$ and $\delta^{2}H$ ($dxs = \delta^{2}H - 8 * \delta^{18}O$) and becomes lower in evaporating water (Dansgaard, 1964). Thus, P — E isometers (low *dxs*, high $\delta^{18}O$) are located on the lower left corner of the distribution that corresponds with dry climates (low P/PE) and strong evaporation effects. The triangular shape of the distribution illustrates that precipitation isometers such as Bison and Jellybean Lakes (high *dxs*, low $\delta^{18}O$), located on the upper area of the distribution, occur in both wet and dry climates (high and low P/PE). In wetter climates, both surface and subsurface through-flow are likely to occur, whereas in drier climates subsurface through-flow may be more common. Between these end-members, represented by the corners of the triangular distribution, are mixed hydrology lakes (intermediate *dxs* and $\delta^{18}O$) for which lake water isotopic composition reflects the combined effects of changes in precipitation-$\delta^{18}O$ and evaporation.

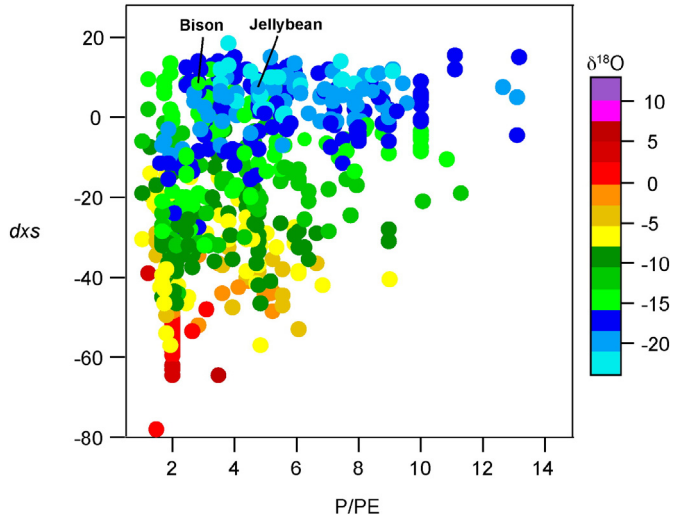

Fig. 4. Lake water deuterium excess (*dxs*) versus NCEP-NARR P/PE color-coded by $\delta^{18}O$ value (Table 1, Supplemental files). Note the trend for lakes to have lower *dxs* in regions of lower P/PE.

3. North Pacific climate controls on precipitation-$\delta^{18}O$ through the Holocene

This review focuses on the two currently available northern and southern precipitation isometers with multi-decadal to century scale resolution that continuously extend from the middle Holocene to the present: Jellybean Lake (hereafter 'JB') located on the east, or leeward, side of the St. Elias Mountains in the southwest Yukon Territory (Anderson et al., 2005, 2007); and Bison Lake, located on a high plateau (~3255 m) in northwest Colorado (Anderson, 2011, 2012; Anderson et al., 2015, 2016). However, first we reassess evidence from proxy and modeling studies regarding climate controls on North Pacific precipitation-$\delta^{18}O$ and the implications for the JB $\delta^{18}O$ interpretation. We then compare the JB and Bison precipitation-$\delta^{18}O$ patterns to draw new conclusions about the role of internal climate modes on western North American hydroclimate.

3.1. Gulf of Alaska atmospheric circulation and precipitation-$\delta^{18}O$

Prior analysis of the JB and the Mount Logan (hereafter 'ML') $\delta^{18}O$ records led to the hypothesis that regional precipitation-$\delta^{18}O$ in the North Pacific Gulf of Alaska region is primarily controlled by atmospheric circulation processes rather than temperature (Anderson et al., 2005; Fisher et al., 2004). The following review will show that subsequent data and modeling studies support this hypothesis, while underscoring considerable uncertainty about specific circulation mechanisms that cause different precipitation-$\delta^{18}O$ shifts and trends through time.

A significant challenge for testing $\delta^{18}O$-climate hypotheses in the North Pacific region is the dearth of historical observational climate and isotopic data. This issue is compounded by the topographic complexity of the area, which leads to significant climatic heterogeneity within small geographic domains. For instance, the extreme topography (e.g., ~3000 to 5000 m a.s.l.) within a few kilometers of the coastline generates substantial climate gradients 50 km farther inland. This physiography also contributes to the shape of the large-scale geostrophic flow across northwestern North America and the existence of the semi-permanent Aleutian Low (AL) pressure center located over the eastern North Pacific (Fig. 5). Due to its mid-latitude position, the AL is influenced by Arctic and subtropical ocean–atmosphere processes, which contribute significant complexity to its temporal and spatial variance. This convergence of diverse and geographically distant controlling factors also highlights why a clearer understanding of the historical and paleoclimate changes of the North Pacific region has broader implications, for both North America and Northern Hemisphere climates.

3.1.1. Empirical evidence

Three central characteristics of the JB and ML records support the original circulation hypothesis, as presented in Fisher et al. (2004), wherein stronger AL and meridional flow results in more depleted precipitation-$\delta^{18}O$ in the southwest Yukon Territory. We term this as the "strong-depleted" hypothesis. These characteristics are: (1) the independently dated lake and ice records exhibit similar multi-decadal trends and shifts over the past 2000 years, with relatively high $\delta^{18}O$ values during most of the Little Ice Age (LIA; Fig. 6), (2) the large negative $\delta^{18}O$ shifts at ~1850 AD at both the ice core elevation (~5000 m) and JB headwater elevation (~1300 m) are consistent with a modeled shift in the vertical $\delta^{18}O$ profile on ML (Holdsworth and Fogarsi, 1991), and (3) the magnitude of JB and ML $\delta^{18}O$ variability and relatively enriched $\delta^{18}O$ values during the LIA are not explained by existing temperature-$\delta^{18}O$ relations, which imply higher temperatures that are

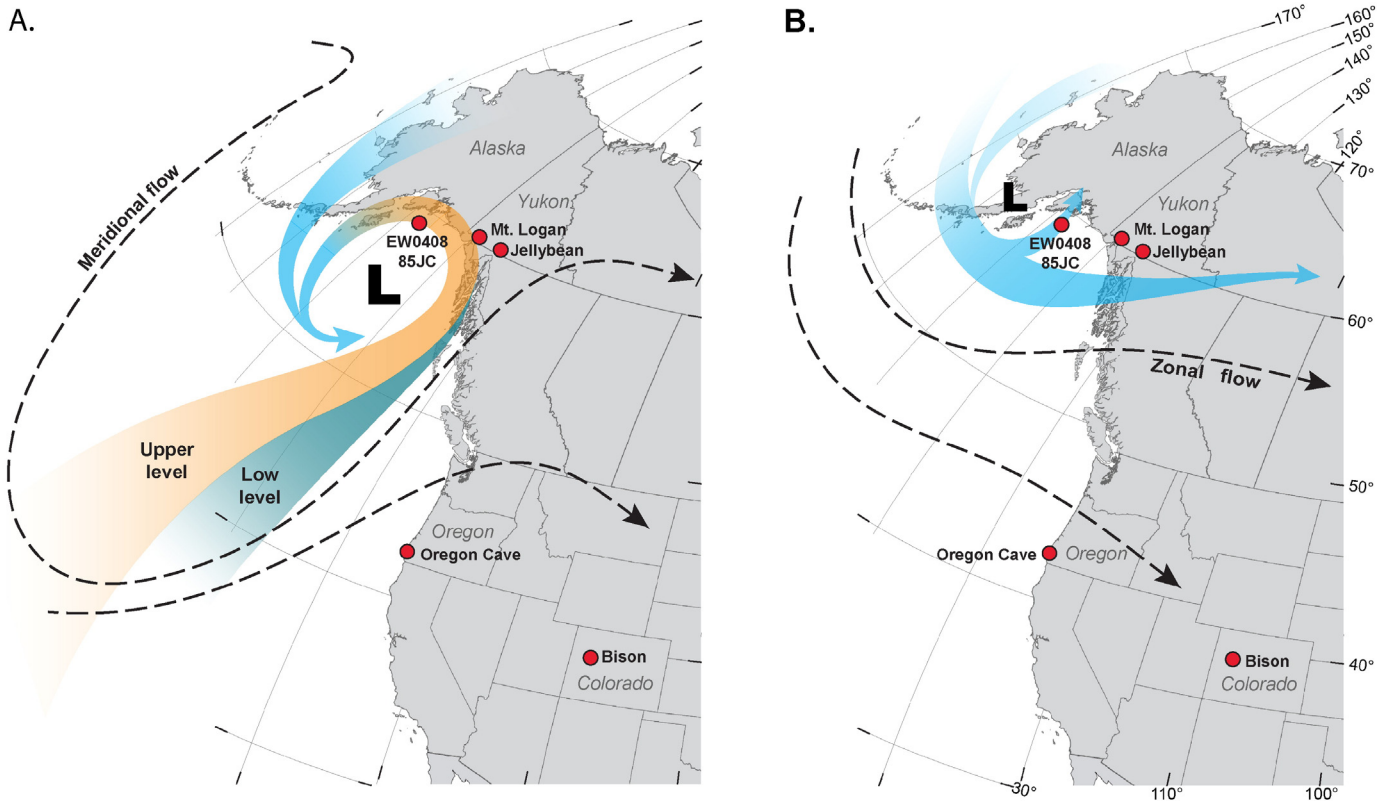

Fig. 5. Schematic of generalized Aleutian Low (the bold L) and jet stream circulation patterns in the northeast Pacific associated with PDO and NPI phases; (A) strong +PDO/−NPI patterns correspond with deep AL centers and cyclonic flow drawing subtropical vapor northward along the west coast of North America and cold Arctic vapor southward. Although strong AL centers are often positioned over the eastern sector of the Gulf of Alaska as shown here, its position varies. Note the strong S-N meridional character of flow; and (B) neutral-to-strong −PDO/+NPI pattern that corresponds with a weak AL center that less vigorously entrains North Pacific vapor eastward within zonal jet stream flow. Historically, the mean east or west position of the AL during such states is highly variable (Rodionov et al., 2007).

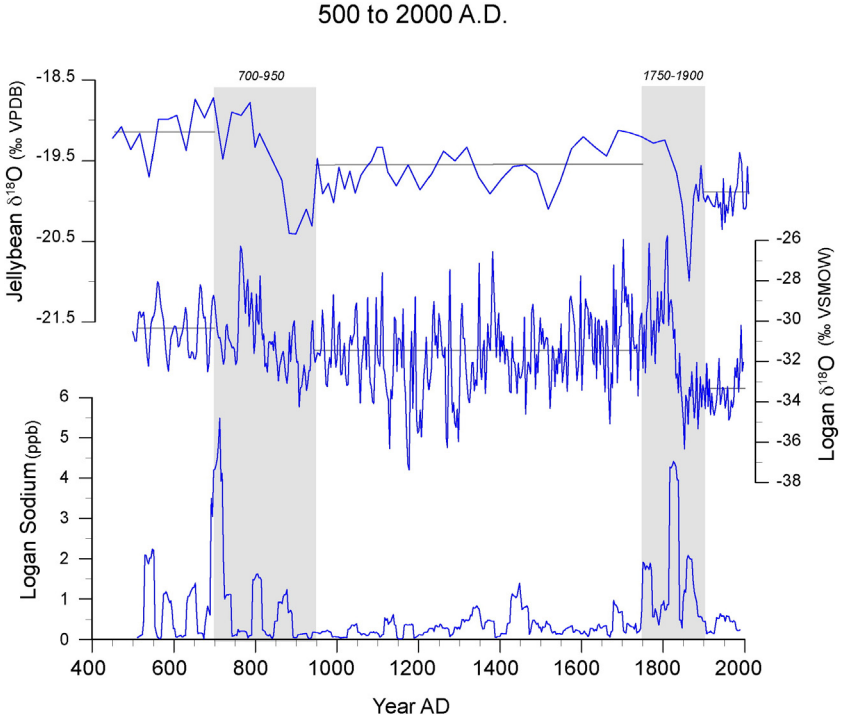

Fig. 6. Jellybean (JB) $\delta^{18}O$ and 3-yr running average of Mount Logan (ML) sodium and $\delta^{18}O$ on an AD scale for the past 1500 years. Gray shaded areas identify prominent negative shifts in $\delta^{18}O$ that correspond to higher sodium concentrations.

inconsistent with colder temperatures inferred from LIA glacier advances. Collectively, these observations indicate that in addition to temperature, North Pacific precipitation-$\delta^{18}O$ is also controlled by the location of the water vapor source, vapor transport distance and rainout effects, and vertical orographic mixing (e.g., Berkelhammer et al., 2011).

Anderson et al. (2005) also proposed that different storm track orientations relative to the coastal mountain barrier would lead to unique changes in precipitation fractionation. Based on modern rain shadow precipitation processes, they asserted that AL intensification and more southerly storm tracks, which produce higher precipitation along the coasts, and higher snow accumulation at higher elevations, subsequently results in greater fractionation and more depleted $\delta^{18}O$ at ML and JB. Anderson et al. (2007) further proposed that the varying storm tracks would affect aridity in the leeward rain-shadow regions and tested this hypothesis with nearby Marcella Lake, a P − E isometer. Rapid Marcella $\delta^{18}O$ increases at ~1850 AD and ~800 BP (1200 AD) indicated shifts to more arid conditions that were coincident with the prominent negative shift to depleted $\delta^{18}O$ values at JB and ML, hypothesized to reflect a stronger AL. Additional support for this hypothesis is provided by two-phase LIA glacier growth (Barclay et al., 2009), pollen assemblages that indicate greater coastal precipitation (Heusser et al., 1985), and similar $\delta^{18}O$ variations at Seven Mile Lake, another P − E isometer, in the central Yukon (Anderson et al., 2011).

Anderson et al. (2005) compared JB-$\delta^{18}O$ and the 100-yr North Pacific Index (NPI) (Trenberth and Hurrell, 1994), a metric of northeastern Pacific sea level pressure (SLP) anomalies that is closely associated with AL strength, and incorrectly reported a positive correlation between depleted JB-$\delta^{18}O$ and negative NPI (strong AL) that was, in fact, an inverse correlation (Fig. 7). Though the inverse correlation was significant ($r^2 = 0.23$, $p < 0.95$), the ^{210}Pb-determined ages have substantial uncertainty (±5 to 20 years) and there are minimal degrees of freedom in the correlation statistic. It is possible to obtain significant positive or negative correlations by tuning the JB $\delta^{18}O$ anomalies within conservative age error estimates and using various NPI smoothing

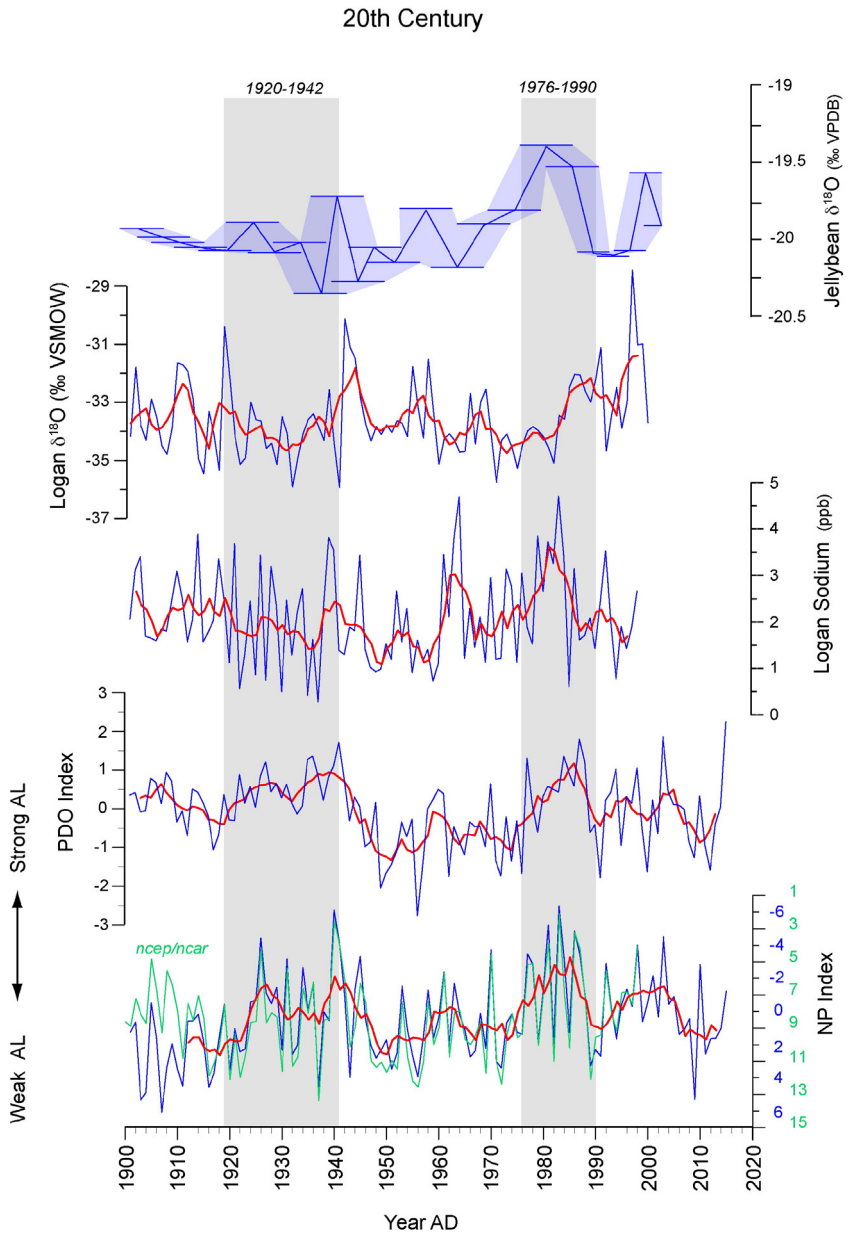

Fig. 7. Time-series: annual (blue) and 5-yr running average (red) of the PDO, NPI (note the reversed scale), ML sodium and $\delta^{18}O$ (Osterberg et al., 2014; Fisher et al., 2004) since 1900 A.D. The JB $\delta^{18}O$ data are shown with a shaded area to outline the ±2 to 5-yr age error estimates. The NPI index is also shown for the NCEP/NCAR re-analyses (green) to illustrate differences prior to 1928. Gray shaded areas identify prominent +PDO/−NPI phases between 1920 to 1942 and 1976 to 1990.

intervals. We now conclude that comparisons between JB $\delta^{18}O$ anomalies and the NPI are ambiguous. In the annually dated ML record, there is a suggestion of a negative correlation between $\delta^{18}O$ and NPI (Fig. 7). However, high noise levels for both of the annual ML ice core $\delta^{18}O$ series (PRC and NWC) limit the correlation between them (0.37), and consequently limits the significance of other correlations with them for this period (David Fisher, written communication). The JB and ML $\delta^{18}O$ records are not well correlated since 1900 AD, though again the JB dating uncertainty further complicates the comparison.

Osterberg et al. (2014) have since provided an independent proxy correlation with the NPI from annual measurements of ML sodium (Na^+) concentrations for the past 1500 years, and their results lend support to the original "strong-depleted" precipitation-$\delta^{18}O$ hypothesis (Figs. 6 and 7). Relying on physical arguments that higher sea salt concentrations are associated with higher near-surface central Pacific wind speeds during strong AL circulation (negative NPI), they find an inverse correlation between higher sodium amounts and negative NPI (strong AL) anomalies ($r = -0.45$, $p < 0.001$). The inverse correlation has the strongest significance with no lead or lag, is relatively insensitive to different winter month NPI sampling, and both variables have similar power spectra. Importantly, rapid increases in both sodium concentrations and variance between ~1820 and 1850 AD coincide with the larger negative shifts to depleted JB and ML $\delta^{18}O$ (Fig. 6). Similarly, the large negative shift to depleted JB and ML $\delta^{18}O$ between ~700 and 800 BP (1200 to 1100 AD) coincides with greater ML sodium variance.

The comparison between ML $\delta^{18}O$ and sodium during the instrumental period further illustrates the aforementioned uncertainty for the ice $\delta^{18}O$ interpretations during the most recent 100-yr time period (Fig. 7). Although higher sodium and depleted $\delta^{18}O$ values during the 1980s positive PDO are consistent with the "strong-depleted" hypothesis, the overall correlation between 3-yr averages of ML sodium and $\delta^{18}O$ since 1900 AD is only weakly negative and not significant ($r^2 = 0.02$). For instance, during the two decades prior to the late 1970s shift from a negative to a positive PDO (positive to negative NPI) phase, lower ML sodium concentrations occurred with depleted $\delta^{18}O$, which contrasts with the aforementioned "strong-depleted" association. The previous positive PDO (negative NPI) phase during the 1920s and 1930s is also not registered strongly by either proxy.

This comparison may also be an illustration of the difficulty in correlating annual ice-$\delta^{18}O$ variations, which exhibit strong seasonal sensitivity to climate metrics. Rupper et al. (2004) show that only in years of high snow accumulation does ML have a robust connection with atmospheric circulation (Moore et al., 2002). Thus, seasonal biases and the low signal-to-noise ratio over the historical period, which are also similar features of JB $\delta^{18}O$, provide likely explanations for weak relationships since 1900 AD between the NPI, and the PDO, and JB and ML $\delta^{18}O$ records. It is important to recognize that pre-20th century ML and JB $\delta^{18}O$ shifts are much larger (~2 to 6‰; Fig. 6), and this highlights that 20th century comparisons and modern analogues are probably insufficient to characterize the full range of Holocene variability.

3.1.2. Model simulations

The first principles of atmospheric circulation dynamics suggest that the "strong-depleted" hypothesis is counterintuitive. This conundrum arises because strong AL circulation is typically observed to entrain greater amounts of sub-tropical moisture composed of vapor derived from relatively warm ocean water (Fig. 5; Papineau, 2001). This is because if all other factors are assumed to be equal, then warmer ocean waters would be expected to produce vapor more enriched in ^{18}O than colder ocean water. Therefore, southerly sourced vapor would be expected to generate more enriched precipitation-$\delta^{18}O$ than that derived from cold, northerly sourced vapor. This effect is robustly reproduced by numerous isotope enabled General Circulation Models (Berkelhammer et al., 2011; Field et al., 2010; Liu et al., 2014; Porter et al., 2013).

Field et al. (2010) and Porter et al. (2013) use the NASA-GISS Model E (Schmidt et al., 2005) configured with a $4° \times 5°$ and $2° \times 2.5°$ horizontal grid resolution, with 45 and 40 vertical levels, respectively. Field et al. (2010) simulated the 45 years since 1954 as an analogue study whereas Porter et al. (2013) simulated the 1970–2009 period nudged by NCEP/NCAR reanalysis data. Both models were forced with interannually varying sea surface temperatures (SSTs) and sea ice fields from the HADISST 1.1 dataset (Rayner et al., 2003). Both GCM simulations provide evidence for strong circulation controls on precipitation-$\delta^{18}O$, with a clear "strong-enriched" AL to precipitation-$\delta^{18}O$ association as well as strong AL circulation controls on precipitation amount and temperature.

Indicating further GCM uniformity, Liu et al. (2014) evaluated precipitation-$\delta^{18}O$ controls by the Pacific North America (PNA) pattern with the Isotopes-incorporated Global Spectral Model (IsoGSM) for 1950–2005 and obtained a similar result. Characterized by a ridge-trough pressure gradient over western North America, a positive PNA is associated with a strong AL, and positive PDO and negative NPI phases. Further insight into the IsoGSM model is provided by Berkelhammer et al. (2011) who examined isotopic anomalies in precipitation for individual years (1989, 1998, and 2003) with contrasting annual circulation and precipitation-$\delta^{18}O$ patterns (Fig. 8). Consistent with Liu et al. (2014), the IsoGSM simulations indicate that strong AL circulation in 1998 and 2003 enhanced southwesterly wind anomalies producing regions of enriched precipitation-$\delta^{18}O$ extending from the subtropics to Alaska that contrast with depleted precipitation-$\delta^{18}O$ throughout western North America during weak AL circulation in 1989.

Fisher et al. (2004) took a different approach, using a numerical regional stable isotope model coupled to a zonally averaged global model to compare a simulated and observed vertical $\delta^{18}O$ profile on ML for vapor sourced from different regions (Fig. 9). Their reasoning was guided by the previously documented vertical $\delta^{18}O$ and *dxs* discontinuity on ML (Holdsworth and Fogarsi, 1991; Holdsworth and Krouse, 2002). The vertical $\delta^{18}O$ discontinuity suggested three atmospheric layers during precipitation on the St. Elias Mountain barrier: (1) a lower monotonic fractionation sequence below ~3 km, (2) a middle mixed layer, typically 1–2 km thick in which $\delta^{18}O$ is nearly constant regardless of altitude, and (3) an upper "quasi geostrophic flow" layer above ~5.3 km with a fractionation sequence isolated from the lowermost layer below 3 km. The implications of this vertical stratification are that upper and lower vapor sources may differ and that changes in the height of the boundary layer could give rise to complex signals of precipitation-$\delta^{18}O$ at different elevations.

The same numerical model had successfully simulated the vertical $\delta^{18}O$ profiles of the Devon ice cap in Arctic Canada, and the Greenland and Antarctic ice sheets (Fisher, 1992). The model also appears to successfully simulate the vertical ML-$\delta^{18}O$ profile, although there are a limited number of calibration points (Fig. 9a). Two different simulations were conducted for (1) subtropical (~20°N) and North Pacific vapor sources (modern, meridional) and (2) only North Pacific vapor sources (zonal). The simulations indicated that the addition of subtropical moisture caused changes to the vertical $\delta^{18}O$ profile, which led to more depleted precipitation-$\delta^{18}O$ at ML and JB elevations that are consistent with the shifts to more depleted $\delta^{18}O$ at ~1850 AD (Figs. 7 and 9b).

3.2. Updated summary of North Pacific precipitation-$\delta^{18}O$

This updated assessment of multiple data types provides a clear consensus for hypothesis regarding atmospheric circulation controls on precipitation-$\delta^{18}O$ in the North Pacific region. Firstly, both the proxy data and models indicate no evidence for dominance by temperature, precipitation amount, or seasonality. However, significant differences between the models and proxy data indicate that the precise circulation mechanism that gives rise to precipitation-$\delta^{18}O$ signals remain ambiguous. We assert that uncertainties regarding boundary layer height are a likely explanation for some of these differences because no existing

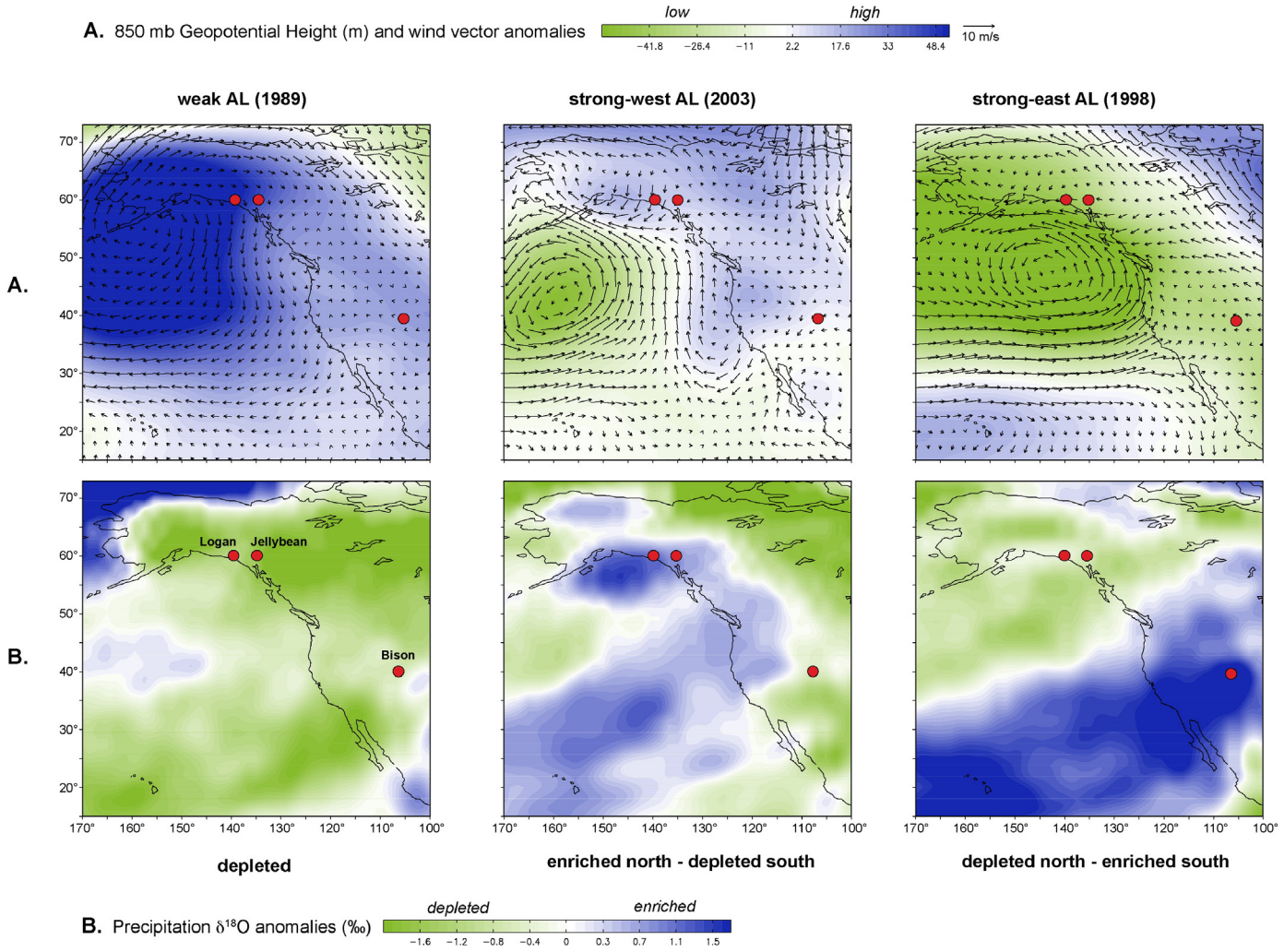

Fig. 8. Modeled precipitation-$\delta^{18}O$ patterns for the North Pacific climate during the winters (NDJFM) of 1989, 2003 and 1998 (from Berkelhammer et al., 2011); the top row (A) shows wind vector and average annual 850 mb geopotential height anomalies (m, green = low, purple = high), and the lower row (B) shows the IsoGSM precipitation-$\delta^{18}O$ anomalies (green = depleted, blue = enriched). A −PDO/+NPI circulation in 1989 illustrates a weak AL, west-northwesterly flow, and depleted precipitation-$\delta^{18}O$ throughout western North America. Two varieties of +PDO/−NPI are illustrated by 2003 and 1998; in 2003 a strong-west AL results in enriched-north/depleted-south precipitation-$\delta^{18}O$ dipole, whereas a strong-east AL in 1998 results in depleted-north/enriched-south precipitation-$\delta^{18}O$ dipole. Note the opposite sign of the precipitation-$\delta^{18}O$ anomalies at JB and Bison Lakes during such circulation patterns.

model simulations explicitly address variations in the height of vertical mixing between the marine boundary layer and upper level geostrophic flow in response to circulation changes. In Hawaii the same mechanisms have been observed to create temporally complex vertical precipitation-$\delta^{18}O$ profiles (Bailey et al., 2013), an observation that raises questions about the rates and heights of mixing and associated fractionations. Further investigation of vertical processes by isotope-enabled model simulations to address the ambiguities identified here, and to examine water resource implications for similar orographic processes in the Pacific Northwest (e.g., Luce et al., 2013), will be crucial to advancing our understanding of regional precipitation-$\delta^{18}O$ controls.

Also clearly missing from the empirical evidence is continuous, observational monitoring of precipitation-$\delta^{18}O$ designed to capture both synoptic-scale events and their response to lower frequency circulation patterns within this topographically complex region. Recent monitoring of U.S. Rocky Mountain snowpack-$\delta^{18}O$ has confirmed that observations over long time periods with high spatial density are necessary to capture complex spatial heterogeneity in mountainous regions (Anderson et al., 2016). The sparse temporal and spatial coverage of the observational precipitation-$\delta^{18}O$ data available from the Global Network of Isotopes in Precipitation (GNIP) may capture broad scale fractionation effects (e.g., Bailey et al., 2015) but is too coarse to capture the isotopic processes required to evaluate local to regional controls. A monitoring network on an elevation gradient across coastal mountain barriers would make a strong contribution to better resolve this uncertainty.

Along these lines, sampling of snowpack $\delta^{18}O$ at Wolverine glacier, located on the Alaskan Kenai Peninsula with an elevation range between ~450 and 1680 m, began in spring of 2014. The sampling followed several rain-on-snow events in late January when persistent southerly atmospheric flow advected unseasonably warm temperatures and subtropical vapor into south-central Alaska. Ice layers associated with this rain event were identified in a snow pit at ~1000 m elevation and $\delta^{18}O$ profiles indicate higher *dxs* and depleted $\delta^{18}O$ (by −4‰) compared with surrounding snow (Shad O'Neel, Eric Klein and Jeff Welker, written communication). If the ice layers do in fact represent the rain event, and not sublimation or some other post-depositional process, then the low $\delta^{18}O$ values support the "strong-depleted" hypothesis. Alternatively, the low values could also reflect boundary layer dynamics for this individual synoptic event that is related to a highly localized orographic rainout process. Additional observations are required to pinpoint more precise causes of spatial and temporal variability in vertical precipitation-$\delta^{18}O$ gradients in mountainous regions.

In summary, although more evidence has been collected, there remains significant uncertainty about atmospheric circulation controls

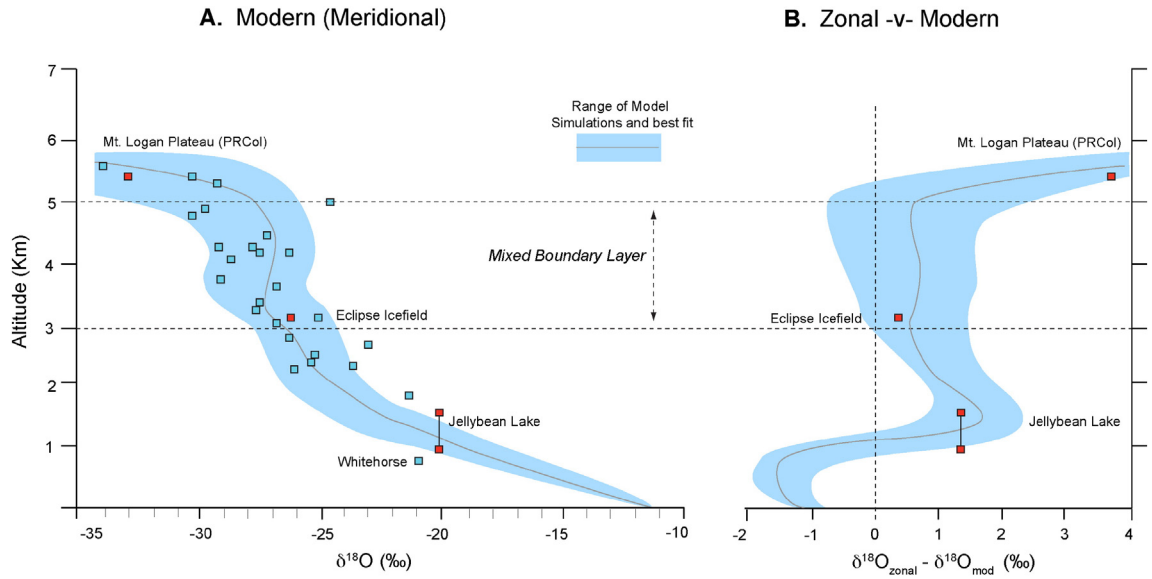

Fig. 9. Vertical precipitation-$\delta^{18}O$ trends for the St. Elias Mountains of southern Yukon Territory and Alaska (from Fisher et al., 2004); the left panel (A) shows the modeled vertical profile (range of model simulations and best fit) and measured data (sources listed in Fisher et al., 2004) interpreted to represent a modern meridional circulation pattern. The right panel (B) shows the modeled effects on the vertical profile shown in (A) for only North Pacific sources estimated for zonal flow. The red squares in (B) are the $\Delta\delta^{18}O$ observed before and after the ~1850 AD shift at ML, Eclipse Icefield (Wake et al., 2003), and JB shown in Fig. 7. The lower JB square is the elevation of the lake and the upper square is the highest elevation of the lake's watershed.

on precipitation-$\delta^{18}O$ in the North Pacific region. This review has described (1) contrasting results between the GCMs and the numerical modeling experiments, and (2) inconsistent results between proxy records during the instrumental period since ~1900 AD. Regarding the first point, the different results obtained by the GCM and numerical models can likely be explained by differences in topographic resolution and vertical mixing and boundary layer dynamics. The GCMs appear to broadly capture first principle physical controls but are not as suitable a tool for testing orographic effects, a task for which the numerical model may be better suited. Therefore, the most probable conclusion that can be drawn is that neither model invalidates the other because their designs evaluate different processes on different spatial scales.

Regarding the second point, the relationship between JB and ML $\delta^{18}O$ and metrics of AL strength during the instrumental period that are inconclusive with respect to the coherent negative JB and ML $\delta^{18}O$ shifts at ~1850 AD and ~800 BP (1200 AD) (Figs. 6 and 7) are most likely related to uncertainties in dating of JB lake sediment and varying seasonal sensitivity and high-frequency noise of the ML ice core. We also recognize inconsistencies between the JB and ML records and the tree-ring derived NPI record of D'Arrigo et al. (2005); yet differences between tree-rings, lake sediments and ice cores can also potentially be understood in the context of unique proxy sensitivity, seasonal biases, and high-frequency noise (Anderson et al., 2011; Osterberg et al., 2014; Steinman et al., 2012). Another approach to better understand patterns of Pacific ocean–atmosphere change is to examine spatially distributed lake sediment-$\delta^{18}O$ through the Holocene from precipitation isometers to develop hypotheses that explain similarities and differences, which is the concluding part of this review.

4. New perspectives on north–south precipitation-$\delta^{18}O$ patterns through the Holocene

As described in Section 2.1, precipitation isometers such as in the case of Bison, Lime, JB, and Tangled Up Lakes, exhibit negligible overprinting by variations in humidity or hydrology. Of these records, JB and Bison extend back to the middle Holocene with multi-decadal to centennial resolution and are geographically positioned to evaluate north–south precipitation-$\delta^{18}O$ variations (Fig. 10). The records have independently established chronologies based on ^{210}Pb (and ^{137}Cs for JB), calibrated ^{14}C ages of terrestrial macrofossils, and late Holocene tephra layers (Anderson et al., 2005; Anderson, 2011, 2012). Their comparison reveals previously unobserved sequences of in-phase and anti-phase precipitation-$\delta^{18}O$ dipole patterns over a range of timescales.

During the middle Holocene (8–4 ka) JB and Bison records share few similarities; JB displays low-frequency cycles of ~1000-yr length with a tendency towards decreasing and depleted $\delta^{18}O$ anomalies, whereas Bison displays a steady multi-millennial decline from highly enriched anomalies. We suggest that these differences resulted from weak mid-Holocene expression of large-scale forcing by Pacific ocean–atmosphere dynamics as we know them today, and that the records instead predominantly indicate stronger regional responses to external forcing. The most prominent external forcing mechanism during the middle Holocene is solar insolation, which influenced each region differently, ranging from summer values 8 to 15% higher-than-present and winter values 8 to 15% lower within the latitude band between ~40° and ~70° of the study sites (Berger and Loutre, 1991). In the southern regions, higher summer solar insolation is thought to have led to an enhanced North American Monsoon (NAM), as suggested by modeling and additional proxy records (Metcalf et al., 2015; Jones et al., 2015). This relationship is consistent with positive Bison anomalies that reflect warmer than average temperature of precipitation and rain dominance of the seasonal precipitation balance (Anderson, 2012; Anderson et al., 2016).

In contrast, millennial-scale JB variations bear a closer similarity to those in carbonate-$\delta^{18}O$ records from the Oregon Cave NM speleothem (Ersek et al., 2012) as well as with a record of near-surface GoA planktonic foraminifera-$\delta^{18}O$ (Praetorius and Mix, 2014). These records are interpreted to reflect winter atmospheric temperature and precipitation, and sea surface temperature (SST) controls, respectively (Fig. 11). Ersek et al. (2012) identified similarities between the Oregon Cave NM speleothem and solar irradiance reconstructions from records of ^{14}C production and ^{10}Be fluxes that are also evident between JB and a combined solar irradiance index (Fig. 10; Steinhilber et al., 2012). Praetorius and Mix (2014) highlight the relative decoupling, or seesaw behavior between Greenland (NGRIP) and GoA during the Holocene in contrast to deglacial

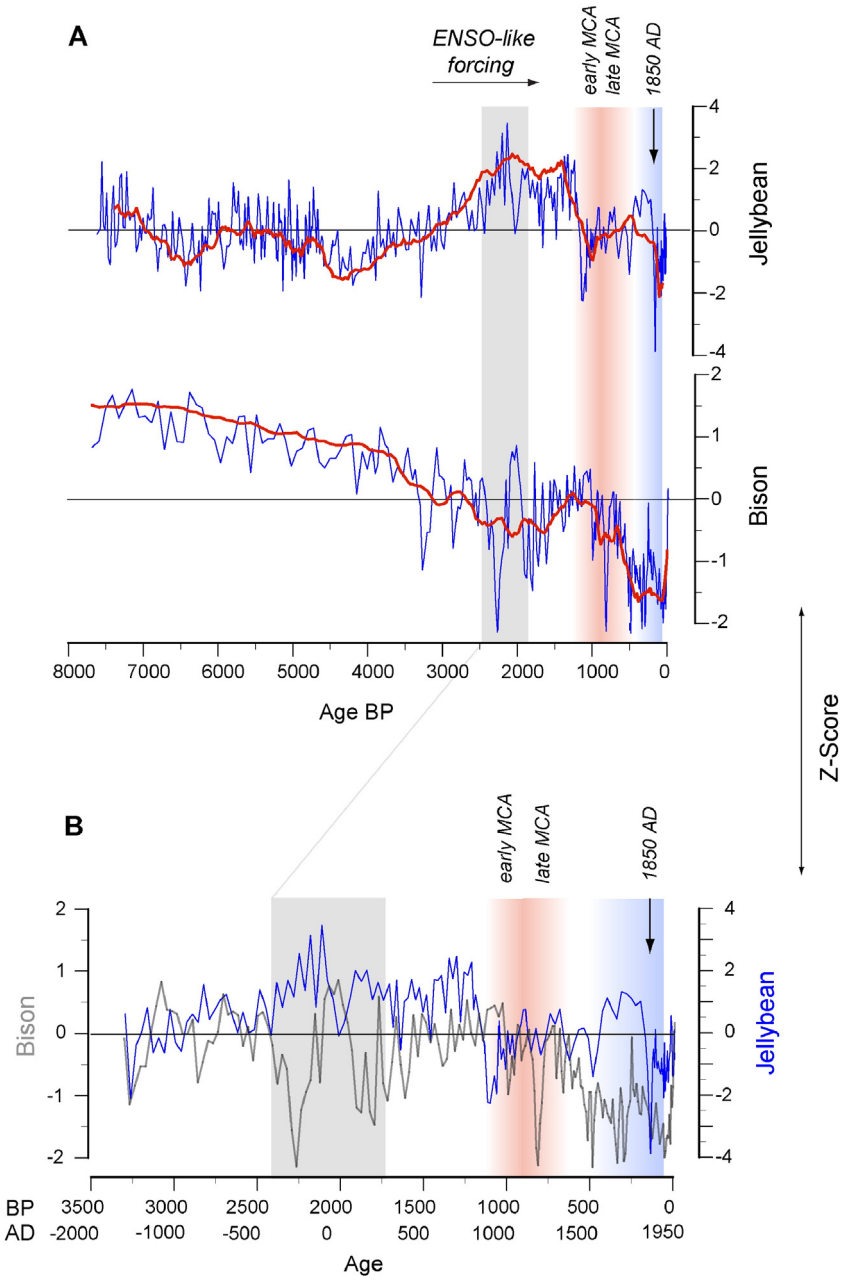

Fig. 10. Holocene JB and Bison Lake $\delta^{18}O$ z-score records over (A) the last 8000 cal years (blue = raw, red = 21-interval smoothing), and (B) expands the past 3500 years on AD and cal yr. BP age scales. The shaded intervals reflect key periods of transition discussed in the text (grey = Bison, blue = JB).

times. However, both of these records also indicate a gradual increase to more enriched $\delta^{18}O$, which is not evident at either JB or ML, which have low-frequency trends towards more depleted $\delta^{18}O$.

Barron and Anderson (2011) suggest that terrestrial and marine proxy data along the northeast Pacific margin indicate the possibility of a more negative PDO/La Niña-like mean-state of the Pacific during the mid-Holocene. However, such an analogy and the implied large-scale teleconnection between weak AL strength and precipitation-$\delta^{18}O$ as either the "weak-enriched" corollary or the "strong-depleted" hypothesis, is inconsistent with the out-of-phase anomalies between JB, Bison, Oregon, and GoA records. We now suggest that these comparisons imply that the North Pacific and AL did not interact with the subtropical Pacific in a coupled PDO/ENSO-like manner during the middle Holocene. In the absence of strong AL coupling with subtropical ocean–atmosphere dynamics during the middle Holocene, it is possible that the AL was more strongly influenced by northern modes of variability (e.g., Northern Annual Mode or Arctic Oscillation) and a North Atlantic forcing component. For instance, if relatively depleted JB $\delta^{18}O$ might predominantly reflect colder, northerly sourced vapor associated with high latitude forcing, then this could reflect an influence by Bering Sea and/or Arctic sea ice extent in addition to millennial scale Arctic circulation processes (Darby et al., 2012; Harada et al., 2014; McKay et al., 2008).

At ~4 ka both JB and Bison begin a millennial scale trend towards an enriched-north/depleted-south dipole precipitation-$\delta^{18}O$ pattern that terminates at ~2 ka, which, for example, is a pattern consistent with a modeled strong-west AL modern analogue (Fig. 8, middle panels). In addition, there are two multi-century anti-phase, depleted-north/enriched-south, dipole patterns between 2.2 and 1.8 ka (Fig. 9), which, for example, are consistent with a modeled strong-east AL modern analogue (Fig. 8, right panels). We suggest that this coupled north–south precipitation-$\delta^{18}O$ dipole behavior, in contrast to the divergent

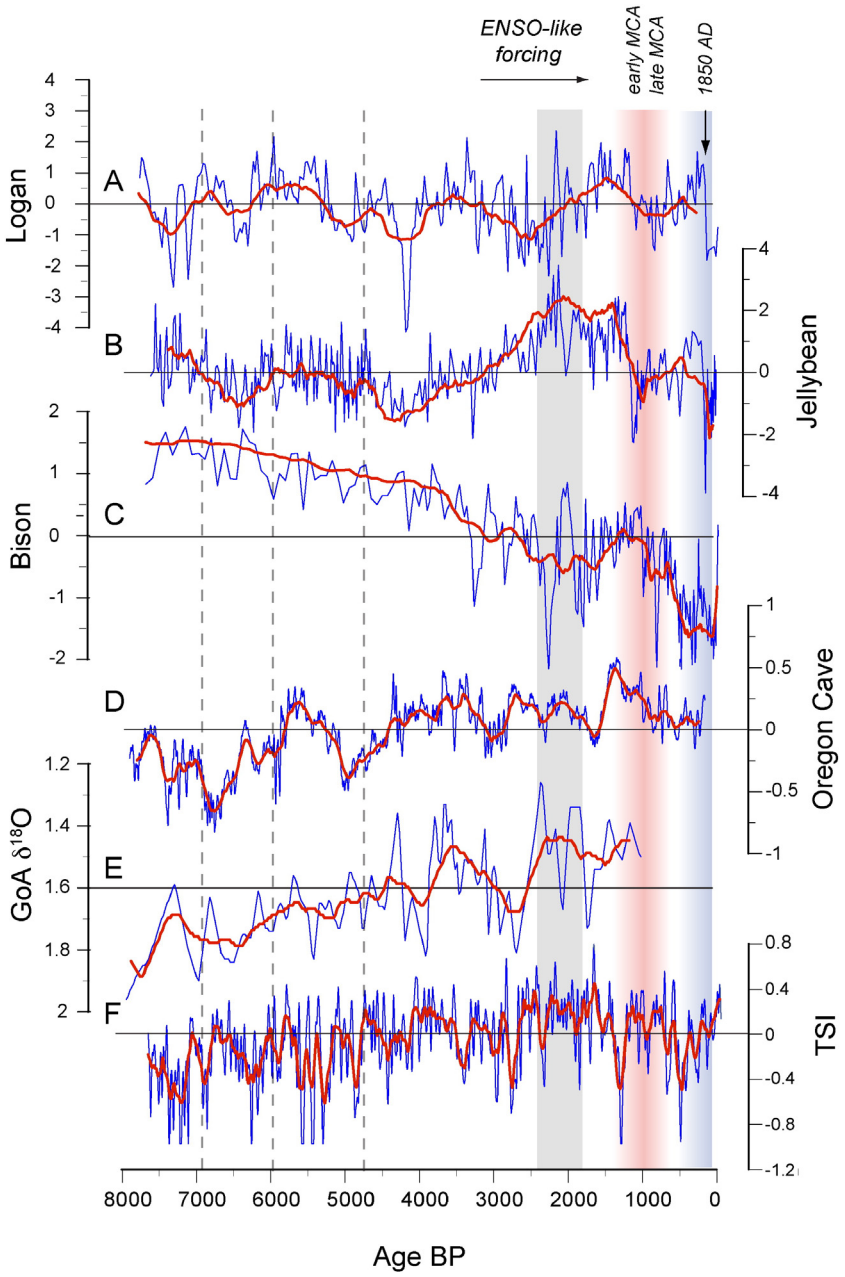

Fig. 11. Holocene z-scores for JB and Bison lake-$\delta^{18}O$, Mount Logan ice-$\delta^{18}O$ (Fisher et al., 2008), and Oregon Cave NM speleothem-$\delta^{18}O$ (Ersek et al., 2012) with Gulf of Alaska foraminifera-$\delta^{18}O$ (‰VPDB; Praetorius and Mix, 2014), and total solar irradiance (TSI) anomalies based on combined ^{10}Be from ice core records and ^{14}C from tree-rings (Steinhilber et al., 2012) (blue = raw, red = 21-interval smoothing with exception of TSI where red = 41-interval smoothing).

patterns during the middle Holocene, represents the onset of a tropical controls on Pacific ocean–atmosphere dynamics, as we know them today. Support for this interpretation is also provided by: (1) warmer alkenone-inferred North Pacific SSTs between ~4 and 3 ka, which suggests northward transport of subtropical waters offshore of northern California and the Gulf of Alaska associated with the North Pacific gyre (Barron et al., 2003; Praetorius et al., 2015), and (2) higher than normal background tropical storm activity in the northwest Pacific attributed to an increase in El Niño frequency (Woodruff et al., 2009). The onset of coupled behavior also coincides with an inferred increase in positive Arctic Oscillation (low pressure) circulation (Darby et al., 2012) between ~3 and 1.2 ka, which in the present day also results in more southerly sourced GoA precipitation.

The depleted Bison $\delta^{18}O$ anomalies between ~3 and 1.2 ka are attributed to predominantly colder than average temperatures and snowfall-dominated precipitation balance (Anderson et al., 2016). However, as discussed above, the processes that could explain the enriched JB $\delta^{18}O$ anomalies are uncertain. If enriched JB $\delta^{18}O$ reflect the predominance of warmer southerly derived vapor (for example 2003 in Fig. 8a), which is counter to the "strong-depleted" hypothesis, then the corresponding enriched-north/depleted-south pattern could possibly be consistent with a strong AL, positive PDO/PNA pattern. Comparative analysis of North American carbonate-$\delta^{18}O$ records distributed on eastern and western sides of the continent, including a "weak-enriched" interpretation of the JB record, suggests that a transition occurred at ~4 ka from more negative to positive PNA conditions (Liu et al., 2014). However, we note that additional evidence from highly depleted Rocky

Mountain snowpack-$\delta^{18}O$ associated with strong zonal flow also suggests that an enriched-north/depleted-south precipitation-$\delta^{18}O$ dipole pattern could possibly be the result of zonal patterns (Anderson et al., 2016).

Notably, between ~4 and 3 ka, the JB and ML $\delta^{18}O$ anomalies also diverge: as JB $\delta^{18}O$ became relatively enriched during this period, ML $\delta^{18}O$ remained relatively depleted (Fig. 11). Barron and Anderson (2011) noted that this locally divergent behavior could reflect weak regional climate forcing. We now suggest this behavior is more likely a result of boundary layer fractionation effects caused by changing atmospheric flow. In this instance either reduced vertical mixing or lower boundary layer height, in response to a change in circulation patterns, could account for relatively depleted $\delta^{18}O$ at ML that are not observed at JB, although this proposition remains to be conclusively supported. Thus, the precise mechanisms for how the enriched-north/depleted-south precipitation-$\delta^{18}O$ dipole pattern between ~3 and 1.2 ka relates to specific Pacific, or Arctic, modern analogue circulation patterns is uncertain. Nevertheless, the appearance of the isotope dipole is consistent with increasing influence by subtropical Pacific ocean–atmosphere processes on the hydroclimate of the western North America Cordillera.

Between ~1.5 and 1.2 ka, the enriched-north/depleted-south precipitation-$\delta^{18}O$ dipole reversed (depleted-north/enriched-south) (Fig. 10). Subsequently, during the early Medieval Climate Anomaly (MCA), by ~1000 AD, north and south regions became roughly neutral and in-phase. Between ~1.2 and 0.8 ka (800 to 1200 AD), a strong enriched-north/depleted-south dipole reestablished within decades before rapidly returning to an in-phase neutral pattern by ~0.5 ka (~1500 AD). Similar decadal-scale reversals and dipole responses are not apparent within any previous time period during the Holocene. Thus, although previous studies have identified the MCA interval as a generally negative-PDO-like period (Mann et al., 2009), the precipitation-$\delta^{18}O$ dipole variations shown here reinforce the likelihood that strong forcing by the Pacific ocean–atmosphere dynamics also included a greater variety of Pacific ocean–atmosphere modes and regional responses than a single modern PDO analogue (e.g., Overland et al., 1999; Bond et al., 2003; Overland and Wang, 2005).

During the LIA (~1500 to 1900 AD), a strong multi-century enriched-north/depleted-south precipitation-$\delta^{18}O$ dipole pattern became reestablished. However, at ~1850 AD prominent shifts to the most depleted values of the Holocene at both JB and Bison likely reflect colder temperatures that are well documented during the late 19th and early 20th centuries. We also note that other strongly depleted anomalies between ~3 and 1.2 ka are also consistent with colder temperatures throughout western North America related to neoglaciation. The ~1850 AD shifts could reflect influence by external factors such as solar minima and resultant teleconnections as suggested by others for Arctic and Atlantic sectors (Gray et al., 2004; Ineson et al., 2011; Ortega et al., 2015). Within a Holocene context, though, these prominent high-frequency precipitation-$\delta^{18}O$ shifts serve to reinforce the notion that complex precipitation-$\delta^{18}O$ behavior exists for a wide range of frequencies, an observation that further informs the aforementioned proxy and modeling discussion.

5. Conclusions

This review has characterized lake $\delta^{18}O$ records from western North America, established their classification as isometers, and shown their utility as tracers of past hydroclimate variability. Lakes that act as precipitation isometers are differentiated from those that act as P − E isometers, and it is shown that comparative analysis of lake $\delta^{18}O$ records are most effective for similar isometer types. The review of past research indicates a clear consensus that internal ocean–atmosphere modes exert strong control on western North American precipitation-$\delta^{18}O$. Prominent north–south precipitation-$\delta^{18}O$ pattern variations indicated by JB and Bison Lakes from the middle Holocene to the present provide evidence for a highly non-stationary influence of Pacific ocean–atmosphere processes on the hydroclimate of western North America.

The north–south precipitation-$\delta^{18}O$ patterns indicate that the internal climate mechanisms such as ENSO, PDO and PNA, that reflect an intrinsically coupled tropical and North Pacific ocean–atmosphere system, became a dominant forcing of hydroclimate in western North America after ~4 ka. Prior to that time, it seems more likely that each region was responding independently to external forcing by solar insolation; northern regions were more strongly influenced by Arctic and Atlantic forcing, including the influence of sea ice extent; whereas the southernmost regions were more strongly influenced by North American Monsoon dynamics. The onset of north–south precipitation-$\delta^{18}O$ patterns suggests that only after ~4 ka did the tropical and North Pacific regions begin to act in a coupled manner to produce climate variability that was unprecedented since the time of deglaciation. These results, combined with previous data and modeling experiments, indicate that we have much to learn about the specific Pacific ocean–atmosphere mechanisms that give rise to different precipitation-$\delta^{18}O$ variations and why their influences vary through time.

This review of western North American lake $\delta^{18}O$ also highlights the importance of obtaining both spatial and temporal information to address questions regarding the timing of regional climate change in response to internal variability and external forcing. The compilation underscores the unlikelihood that a single climate proxy record can provide information for a single climate mode or that is specifically relevant to all areas, especially within a large region of complex topography. Rather, it illustrates the necessity of applying multiple records to identify the numerous processes that cause climate change in western North America. Thus, future efforts should focus on providing additional spatially distributed precipitation-$\delta^{18}O$ and P − E lake records from locations that broaden regional representation.

Furthermore, by selectively comparing proxy records that reflect the same climate component, in this case precipitation-$\delta^{18}O$, we show the utility of a common-data synthesis approach, wherein records that reflect one component of the climate system are compared with one another to provide a foundation for comparison against other proxy types that reflect different climate variables. For instance, a P − E isometer approach utilizing Holocene length records that include Paradise and Cleland Lakes, as well as the inclusion of the previously mentioned proxy records from the Great Basin, Sierra Nevada, and southern California (Kirby et al., 2013) will broaden the perspectives identified here.

Lastly, the impact of new lake carbonate-$\delta^{18}O$ records will only be as great as new insights gained from parallel research on the processes that connect climate variations to precipitation-$\delta^{18}O$ and lake water-$\delta^{18}O$ variations on local to regional scales. Western North American hydroclimate is characterized by the interaction between ocean–atmosphere circulation controls and complex topography, and it is essential that future and existing paleorecords be informed by observational process studies that address the varying effects of vapor source, transport distances, and orographic boundary layer dynamics on precipitation-$\delta^{18}O$ in three dimensions on fine spatial and temporal scales.

Acknowledgments

The U.S. Geological Survey (USGS) Climate and Land Use Change Research and Development supported this research by Anderson and Barron. The National Science Foundation provided support for Berkelhammer (AGS 1502776), Steinman and Abbott (EAR 090220) and Finney (ARC 0909310, AGS 040206). We appreciate assistance by Paco VanSistine and Jeremy Havens with GIS and figures, Dan Engstrom for radiometric dating interpretations, Shad O'Neel, Eric Klein and Jeff Welker for sharing the 2014 Wolverine snow pit data, David Fisher for sharing the Mount Logan data, Alisa Mast for sharing lake water isotope data from the Flat Tops Wilderness of Colorado, and Nathan Stansell for assistance with lake water collections. We thank Matthew Jones, Natalie

Kehrwald and an anonymous reviewer for constructive and helpful comments that greatly improved the manuscript. Any use of trade, product, or firm names is for descriptive purposes only and does not imply endorsement by the U.S. Government.

Appendix A. Supplementary data

Supplementary data associated with this article include a table of the compiled lake water isotope data (.xls), an associated Google map (.kmz), and regional plots with linear regressions (.doc) that can be found in the online version at http://dx.doi.org/10.1016/j.gloplacha.2015.12.021.

References

Abatzoglou, J.T., 2011. Influence of the PNA on declining mountain snowpack in the western United States. Int. J. Climatol. 31, 1135–1142.

Alder, J.R., Hostetler, S.W., 2014. Global climate simulations at 3000 year intervals for the last 21,000 years with the GENMOM coupled atmosphere–ocean model. Clim. Past Discuss. 10, 2925–2978. http://dx.doi.org/10.5194/cpd-2925-2014.

Anderson, L., Abbott, M.B., Finney, B.P., 2001. Holocene climate inferred from oxygen isotope ratios in lake sediments, central Brooks Range. Alaska. Quat. Res. 55, 313–321.

Anderson, L., Birks, J., Rover, J., Guldager, N., 2013. Controls on recent Alaskan lake changes identified from water isotopes and remote sensing. Geophys. Res. Lett. 40, 3413–3418. http://dx.doi.org/10.1002/grl.50672.

Alexander, M., 2010. Extra tropical air–sea interaction, sea surface temperature variability, and the Pacific Decadal Oscillation. In: Sun, D., Bryan, F. (Eds.), Climate Dynamics: Why Does Climate Vary?American Geophysical Union, Washington D.C., pp. 123–148.

Anderson, L., 2011. Holocene record of precipitation seasonality from lake calcite $\delta^{18}O$ in the central Rocky Mountains, United States. Geology 39, 211–214. http://dx.doi.org/10.1130/G31575.31571.

Anderson, L., 2012. Rocky Mountain Hydroclimate: Holocene variability and the role of insolation, ENSO, and the North American Monsoon. Glob. Planet. Chang. 92-93, 198–208.

Anderson, L., Abbott, M.B., Finney, B.P., Burns, S.J., 2005. Regional atmospheric circulation change in the north Pacific during the Holocene inferred from lacustrine carbonate oxygen isotopes, Yukon Territory, Canada. Quat. Res. 64, 21–35 (Errata 65(2006), 350–351).

Anderson, L., Abbott, M.B., Finney, B.P., Burns, S.J., 2007. Late Holocene moisture balance variability in the southwest Yukon Territory, Canada. Quat. Sci. Rev. 26, 130–141.

Anderson, L., Finney, B.P., Shapley, M.D., 2011. Lake carbonate-$\delta^{18}O$ records from the Yukon Territory, Canada: Little Ice Age moisture variability and patterns. Quat. Sci. Rev. 30, 887–898.

Anderson, L., Brunelle, A., Thompson, R.S., 2015a. A multi-proxy record of hydroclimate, vegetation, fire, and post-settlement impacts for a subalpine plateau, central Rocky Mountains, U.S.A. The Holocene 25, 932–943.

Anderson, L., Berkelhammer, M.B., Mast, M.A., 2016. Isotopes in North American Rocky Mountain Snowpack 1993–2014. Quat. Sci. Rev. 131 (Part B), 262–273.

Bailey, A., Toohey, D., Noone, D., 2013. Characterizing moisture exchange between the Hawaiian convective boundary layer and free troposphere using stable isotopes in water. J. Geophys. Res. Atmos. 118, 8208–8221. http://dx.doi.org/10.1002/jgrd.50639.

Bailey, H.L., Kaufman, D., Henderson, A.K., Leng, M.J., 2015. Synoptic scale controls on the $\delta^{18}O$ in precipitation across Beringia. Geophys. Res. Lett. 42. http://dx.doi.org/10.1002/2015GL063983.

Barclay, D.J., Wiles, G.C., Calkin, P.E., 2009. Holocene glacier fluctuations in Alaska. Quat. Sci. Rev. 28, 2034–2048.

Barnett, T.P., Pierce, D.W., 2009. Sustainable water deliveries from the Colorado River in a changing climate. Proc. Natl. Acad. Sci. 106, 7334–7338.

Barron, J., Anderson, L., 2011. Enhanced Late Holocene ENSO/PDO expression along the margins of the Eastern North Pacific. Quat. Int. 235, 3–12.

Barron, J.A., Heusser, L., Herbert, T., Lyle, M., 2003. High-resolution climatic evolution of coastal northern California during the past 16,000 years. Paleoceanography 18, 1020. http://dx.doi.org/10.1029/2002PA000768.

Bartlein, P.J., Hostetler, S.W., Alder, J.R., 2014. Paleoclimate. In: Ohring, G. (Ed.), Climate Change in North America, Regional Climate Studies. Springer International Publishing, Cham Heidelberg New York Dordrecht London, pp. 1–55 http://dx.doi.org/10.1007/1978-1003-1319-03768-03764.

Benson, L., Kashgarian, M., Rye, R., Lund, S., Paillet, F., Smoot, J., Kester, C., Mensing, S., Meko, D., Lindström, S., 2002. Holocene multidecadal and multicentennial droughts affecting Northern California and Nevada. Quat. Sci. Rev. 21, 659–682.

Benson, L., Linsley, B., Smoot, J., Mensing, S., Lund, S., Stine, S., Sarna-Wojcicki, A., 2003. Influence of the Pacific Decadal Oscillation on the climate of the Sierra Nevada, California and Nevada. Quat. Res. 59, 151–159.

Berger, A., Loutre, M.F., 1991. Insolation values for the climate of the last 10 million years. Quat. Sci. Rev. 10, 297–317.

Berkelhammer, M.B., Stott, L.D., Yoshimura, K., Johnson, K., Sinha, A., 2011. Synoptic and mesoscale controls on the isotopic composition of precipitation in the western United States. Clim. Dyn. http://dx.doi.org/10.1007/s00382-00011-01262-00383.

Bond, N.A., Overland, J.E., Spillane, M., Stabeno, P., 2003. Recent shifts in the state of the North Pacific. Geophys. Res. Lett. 30, 2183. http://dx.doi.org/10.1029/2003GL018597 (012003).

Bowen, G.J., Wilkinson, B., 2002. Spatial distribution of $\delta^{18}O$ in meteoric precipitation. Geology 30, 315–318.

Brown, D.P., 2011. Winter circulation anomalies in the western United States associated with antecedent and decadal ENSO variability. Earth Interact. 15, 1–12.

Brown, D.P., Comrie, A.C., 2004. A winter precipitation 'dipole' in the western United States associated with multi-decadal ENSO variability. Geophys. Res. Lett. 31 http://dx.doi.org/10.1029/2003GL018726.

Byrne, J.M., Berg, A., Townshend, I., 1999. Linking observed and general circulation model upper air circulation patterns to current and future snow runoff for the Rocky Mountains. Water Resour. Res. 35, 3793–3802.

Cayan, D.R., Dettinger, M.D., Diaz, H.F., Graham, N.E., 1998. Decadal variability of precipitation over western North America. J. Clim. 11, 3148–3166.

Changnon, D., McKee, T.B., Doesken, N.J., 1993. Annual snowpack patterns across the Rockies: long-term trends and associated 500-mb synoptic patterns. Mon. Weather Rev. 121, 633–647.

Clark, M.P., Serreze, M.C., McCabe, G.J., 2001. Historical effects of El Nino and La Nina events on the seasonal evolution of the montane snowpack in the Columbia and Colorado River Basins. Water Resour. Res. 37, 741–757.

Clegg, B.F., Hu, F.S., 2010. An oxygen-isotope record of Holocene climate change in the south-central Brooks Range, Alaska. Quat. Sci. Rev. 29, 928–939.

Cobb, K.M., Westphal, N., Sayani, H.R., Watson, J.T., Di Lorenzo, E., Cheng, H., Edwards, L.R., Charles, C.D., 2013. Highly variable El Niño-Southern Oscillation throughout the Holocene. Science 339, 67–70. http://dx.doi.org/10.1126/science.1228246.

Collins, M., 2005. El Niño- or La Niña-like climate change? Clim. Dyn. 24, 89–104. http://dx.doi.org/10.1007/s00382-00004-00478-x.

Dansgaard, W., 1964. Stable isotopes in precipitation. Tellus 16, 436–468.

Darby, D., Ortiz, J.D., Grosch, C.E., Lund, S.P., 2012. 1,500-yr cycle in the Arctic Oscillation identified in Holocene Arctic sea-ice drift. Nat. Geosci. 5. http://dx.doi.org/10.1038/ngeo1629.

Darling, G.W., Bath, A.H., Gibson, J.J., Rozanski, K., 2006. Isotopes in water. In: Leng, M.J. (Ed.), Isotopes in Palaeoenvironmental Research. Springer, The Netherlands, pp. 1–66.

D'Arrigo, R., Wilson, R., Deser, C., Wiles, G., Cook, E., Villalba, R., Tudhope, A., Cole, J., Linsley, B., 2005. Tropical–north Pacific climate linkages over the past four centuries. J. Clim. 18, 5253–5265.

Deser, C., Knutti, R., Soloman, S., Phillips, A.S., 2012. Communication of the role of natural variability in future North American climate. Nat. Clim. Chang. 2. http://dx.doi.org/10.1038/nclimate1562.

Dettinger, M., Cayan, D.R., Diaz, H.F., Meko, D.M., 1998. North–south precipitation patterns in western North America on interannual to decadal timescales. J. Clim. 11, 3095–3111.

Ersek, V., Clark, P.U., Mix, A.C., Cheng, H., Edwards, L.R., 2012. Holocene winter climate variability in mid-latitude western North America. Nat. Commun. 3, 1219. http://dx.doi.org/10.1038/ncomms2222.

Field, R.D., Moore, G.W.K., Holdsworth, G., Schmidt, G.A., 2010. A GCM-based analysis of circulation controls on $\delta^{18}O$ in the southwest Yukon, Canada: implications for climate reconstructions in the region. Geophys. Res. Lett. 37, L05706. http://dx.doi.org/10.1029/2009GL041408.

Fisher, D.A., 1992. Stable isotope simulations using a regional stable isotope model coupled to a zonally averaged global model. Cold Reg. Sci. Technol. 21, 61–77.

Fisher, D.A., Wake, C., Kreutz, K., Yalcin, K., Steig, E., Mayewski, P., Anderson, L., Zheng, J., Rupper, S., Zdanowicz, C., Demuth, M., Waszkiewicz, M., Dahl-Jensen, D., Goto-Azuma, K., Bourgeois, J.B., Koerner, R.M., Sekerka, J., Osterberg, E., Abbott, M.B., Finney, B.P., Burns, S.J., 2004. Stable isotope records from Mount Logan, eclipse ice cores and nearby jellybean lake. Water cycle of the North Pacific over 2000 years and over five vertical kilometers: sudden shifts and tropical connections. Géog. Phys. Quatern. 58, 337–352.

Fisher, D., Osterberg, E., Dyke, A., Dahl-Jensen, D., Demuth, M., Zdanowicz, C., Bourgeois, J., Koerner, R.M., Mayewski, P., Wake, C., Kreutz, K., Steig, E., Zheng, J., Yalcin, K., Goto-Azuma, K., Luckman, B., Rupper, S., 2008. The Mt Logan Holocene–late Wisconsinan isotope record: tropical Pacific–Yukon connections. The Holocene 18, 667–677.

Friedman, I., O'Neil, J.R., 1977. Compilation of stable isotope fractionation factors of geochemical interest. U.S. Geological Survey Professional Paper 440-KK, pp. 1–40.

Gat, J.R., 1995. Stable isotopes of fresh and saline lakes. In: Lerman, A. (Ed.), Physics and Chemistry of Lakes. Elsevier, Amsterdam, pp. 139–165.

Gibson, J.J., Birks, S.J., Yi, Y., 2016. Stable isotope mass balance in lakes: a contemporary perspective. Quat. Sci. Rev. 131 (Part B), 316–328.

Gray, S.T., Graumlich, L.J., Betancourt, J.L., Pederson, G.T., 2004. A tree-ring based reconstruction of the Atlantic Multidecadal Oscillation since 1567 A.D. Geophys. Res. Lett. 31. http://dx.doi.org/10.1029/2004GL019932.

Harada, N., Katsuki, K., Nakagawa, M., Matsumoto, A., Seki, O., Addison, J.A., Finney, B.P., Sato, M., 2014. Holocene sea surface temperature and sea ice extent in the Okhotsk and Bering Seas. Prog. Oceanogr. 126, 242–253.

Harrison, S.P., Bartlein, P.J., Brewer, S., Prentice, I.C., Boyd, M., Hessler, I., Holmgren, K., Izumi, K., Willis, K., 2014. Climate model benchmarking with glacial and mid-Holocene climates. Clim. Dyn. 43, 671–688. http://dx.doi.org/10.1007/s00382-00013-01922-00386.

Harrison, S.P., Bartlein, P.J., Izumi, K., Annan, J., Hargreaves, J., Braconnot, P., Kageyama, M., 2015. Evaluation of CMIP5 palaeo-simulation to improve climate projections. Nat. Clim. Chang. http://dx.doi.org/10.1038/nclimate2649.

Henderson, A.K., Shuman, B.N., 2009. Hydrogen and oxygen isotopic compositions of lake water in the western United States. Geol. Soc. Am. Bull. 121, 1179–1189. http://dx.doi.org/10.1130/B26441.26441.

Heusser, C.J., Heusser, L.E., Peteet, D.M., 1985. Late-Quaternary climatic change on the American North Pacific Coast. Nature 315, 485–487.

Hoerling, M., Eischeid, J.K., Perlwitz, J., 2010. Regional precipitation trends: distinguishing natural variability from anthropogenic forcing. J. Clim. 23, 2131–2145.
Holdsworth, G., Fogarsi, S., 1991. Variation of the stable isotopes of water with altitude in the Saint Elias Mountains of Canada. J. Geophys. Res. 96, 7483–7494.
Holdsworth, G., Krouse, R., 2002. Altitudinal variations of the stable isotopes of snow in regions of high relief. J. Glaciol. 48, 31–41.
Ineson, S., Scaife, A.A., Knight, J.R., Manners, J.C., Dunstone, N.J., Gray, L.L., Haigh, J.D., 2011. Solar forcing of winter climate variability in the Northern Hemisphere. Nat. Geosci. 4. http://dx.doi.org/10.1038/ngeo1282.
Ingraham, N.L., 1998. Isotopic variations in precipitation. In: McDonnell, J.J., Kendall, C.K. (Eds.), Isotope Tracers in Catchment Hydrology. Elsevier, Amsterdam, pp. 87–118.
Ito, E., 2001. Application of stable isotope techniques to inorganic and biogenic carbonates. In: Last, W.M., Smol, J.P. (Eds.), Tracking Environmental Change Using Lake Sediments, pp. 351–371.
Jones, M.D., Metcalf, S.E., Davies, S.J., Noren, A., 2015. Late Holocene reorganization and the North American Monsoon. Quat. Sci. Rev. 124, 290–295.
Kendall, C., Coplen, T.B., 2001. Distribution of oxygen-18 and deuterium in river waters across the United States. Hydrol. Process. 15, 1363–1393.
Kirby, M.E., Feakins, S.J., Bonuso, N., Fantozzi, J.M., Hiner, C.A., 2013. Latest Pleistocene to Holocene hydroclimate from Lake Elsinore. Quat. Sci. Rev. 76, 1–15.
Koutavas, A., Joanides, S., 2012. El Niño-Southern Oscillation extrema in the Holocene and Last Glacial Maximum. Paleoceanography 27. http://dx.doi.org/10.1029/2012PA002378.
Lachniet, M.S., Dennison, R.F., Asmerom, Y., Polyak, V., 2014. Orbital control of western North America atmospheric circulation and climate over two glacial cycles. Nat. Commun. 5, 3805. http://dx.doi.org/10.1038/ncomms4805.
Leng, M.J., Marshall, J.D., 2004. Palaeoclimate interpretation of stable isotope data from lake sediment archives. Quat. Sci. Rev. 23, 811–831.
Leng, M.J., Lamb, A.L., Heaton, T.H.E., Marshall, J.D., Wolfe, B.B., Jones, M.D., Holmes, J.A., Arrowsmith, C., 2006. Isotopes in lake sediments. In: Leng, M.J. (Ed.), Isotopes in Palaeoenvironmental Research. Springer, The Netherlands.
L'Heureux, M.L., Mann, M.E., Cook, B.I., Gleason, B.E., Vose, R.S., 2004. Atmospheric circulation influences on seasonal precipitation patterns in Alaska during the latter 20th century. J. Geophys. Res. 109, D06106. http://dx.doi.org/10.1029/2003JD003845.
Li, J., Xie, S., Cook, E.R., Huang, G., D'Arrigo, R., Liu, F., Ma, J., Zheng, X., 2011. Interdecadal modulation of El Niño amplitude during the past millennium. Nat. Clim. Chang. 1. http://dx.doi.org/10.1038/nclimate1086.
Liu, Z., Yoshimura, K., Bowen, G.J., Buenning, N.H., Risi, C., Welker, J.M., Yuan, F., 2014. Paired oxygen isotope records reveal modern North American atmospheric dynamics during the Holocene. Nat. Commun. 5 http://dx.doi.org/10.1038/ncomms4701.
Luce, C.H., Abatzoglou, J.T., Holden, Z.A., 2013. The missing mountain water: slower westerlies decrease orographic enhancement in the Pacific Northwest. Science 342, 1360–1364. http://dx.doi.org/10.1126/science.1242335.
Mann, M.E., Zhang, Z., Rutherford, S., Bradley, R.S., Hughes, M.K., Shindell, D., Amman, C., Faluvegi, G., Ni, F., 2009. Global signatures and dynamical origins of the Little Ice Age and Medieval Climate Anomaly. Science 326, 1256–1260.
McCabe, G.J., Wolock, D.M., 2009. Recent declines in western U.S. snowpack in the context of twentieth-century climate variability. Earth Interact. 13. http://dx.doi.org/10.1175/2009EI283.1.
McCabe-Glyn, S., Johnson, K.R., Strong, C., Berkelhammer, M.B., Sinha, A., Cheng, H., Edwards, L.R., 2013. Variable North Pacific influence on drought in southwestern North America since AD 854. Nat. Geosci. 6, 617–621. http://dx.doi.org/10.1038/ngeo1862.
McKay, J.L., de Vernal, A., Hillaire-Marcel, C., Not, C., Polyak, L., Darby, D., 2008. Holocene fluctuations in Arctic sea-ice cover: dinocyst-based reconstructions for the eastern Chukchi Sea. Can. J. Earth Sci. 45, 1377–1397.
Mesinger, F., Dimego, G., Kalney, E., Mitchell, K., Shafran, P.C., Ebisuzaki, W., Jovic, W., Woollen, D., Roger, E., Berbery, E.H., Ek, M.B., Fan, Y., Grumbine, R., Higgins, W., Li, H., Lin, Y., Manikin, G., Parrish, D., Shi, W., 2006. North American regional reanalysis. Bull. Am. Meteorol. Soc. 87, 343–360.
Metcalf, S.E., Barron, J.A., Davies, S.J., 2015. The Holocene history of the North American Monsoon: 'known knowns' and 'known unknowns' in understanding its spatial and temporal complexity. Quat. Sci. Rev. 120, 1–27.
Miyasaka, T., Nakamura, H., Taguchi, B., Nonaka, M., 2014. Multidecadal modulations of the low-frequency climate variability in the wintertime North Pacific since 1950. Geophys. Res. Lett. 41, 2948–2955. http://dx.doi.org/10.1002/2014GL059696.
Moore, G.W.K., Holdsworth, G., Alverson, K., 2002. Climate change in the North Pacific region over the past three centuries. Nature 420, 401–403.
Mote, P.W., 2006. Climate-driven variability and trends in mountain snowpack in western North America. J. Clim. 19, 6209–6220.
Moy, C.M., Seltzer, G.O., Rodbell, D.T., Anderson, D.M., 2002. Variability of El Niño/Southern Oscillation activity at millennial timescales during the Holocene epoch. Nature 420, 162–165.
Nelson, D.B., Abbott, M.B., Steinman, B., Polissar, P.J., Stansell, N.D., Ortiz, J.D., Rosenmeier, M.F., Finney, B.P., Riedel, J., 2011. Drought variabilitiy in the Pacific Northwest from a 6,000-yr lake sediment record. Proc. Natl. Acad. Sci. 108. http://dx.doi.org/10.1073/pnas.1009194108.
Ortega, P., Lehner, F., Swingedourw, D., Masson-Delmotte, V., Raible, C.C., Casado, M., Yiou, P., 2015. A model-tested North Atlantic Oscillation reconstruction for the past millennium. Nature 523 http://dx.doi.org/10.1038/nature14518.
Osterberg, E., Mayewski, P., Fisher, D., Kreutz, K., Maasch, K.A., Sneed, S.B., Kelsey, E., 2014. Mount Logan ice core record of tropical and solar influences on Aleutian Low variability. J. Geophys. Res. Atmos. 119. http://dx.doi.org/10.1002/2014JD021847.
Overland, J.E., Adams, J.M., Bond, N.A., 1999. Decadal variability of the Aleutian Low and its relation to high-latitude circulation. J. Clim. 12, 1542–1548.
Overland, J.E., Wang, M., 2005. The third Arctic climate pattern, 1930's and early 2000's. Geophys. Res. Lett. 32, L23808. http://dx.doi.org/10.1029/2005GL024254.
Overland, J., Rodionov, S., Minobe, S., Bond, N., 2008. North Pacific regime shifts: definitions, issues and recent transitions. Prog. Oceanogr. 77, 92–102.
Papineau, J.M., 2001. Wintertime temperature anomalies in Alaska correlated with ENSO and PDO. Int. J. Climatol. 21, 1577–1592.
Pederson, G.T., Gray, S.T., Ault, T., Marsh, W., Fagre, D.B., Bunn, A.G., Woodhouse, C.A., Graumlich, L.J., 2011. Climatic controls on snowmelt hydrology of the Northern Rocky Mountains. J. Clim. 24. http://dx.doi.org/10.1175/2010JCL13729.13721.
Pederson, G.T., Betancourt, J.L., McCabe, G.J., 2013. Regional patterns and proximal causes of the recent snowpack decline in the Rocky Mountains, U.S. Geophys. Res. Lett. 40, 1811–1816. http://dx.doi.org/10.1002/grl.50424.
Porter, T.J., Pisaric, M.F.J., Field, R.D., Kokelj, S.V., Edwards, T.W.D., deMontigny, P., Healy, R., LeGrande, A.N., 2013. Spring-summer temperatures since AD 1780 reconstructed from stable oxygen isotope ratios in white spruce tree-rings from the Mackenzie Delta, northwestern Canada. Clim. Dyn. 42, 771–785.
Praetorius, S.K., Mix, A.C., 2014. Synchronization of North Pacific and Greenland climates preceded abrupt deglacial warming. Science 345, 444–448.
Praetorius, S.K., Mix, A.C., Davies, M.H., Wolhowe, M.D., Prahl, F.G., 2015. North Pacific deglacial hypoxic events linked to abrupt ocean warming. Nature 527, 362–366. http://dx.doi.org/10.1038/nature15753.
Rayner, N.A., Parker, D.E., Horton, E.B., 2003. Global analyses of sea surface temperature, sea ice, and night marine air temperature since the late nineteenth century. J. Geophys. Res. 108. http://dx.doi.org/10.1029/2002DJ002670.
Ricketts, R.D., Anderson, R.F., 1998. A direct comparison between the historical record of lake level and the $\delta^{18}O$ signal in carbonate sediments from Lake Turkana, Kenya. Limnol. Oceanogr. 43, 811–822.
Rodionov, S.N., Bond, N.A., Overland, J.A., 2007. The Aleutian Low, storm tracks, and winter climate variability in the Bering Sea. Deep-Sea Res. II 54, 2560–2577.
Rozanski, K., Araguas-Araguas, L., Gonfiantini, R., 1993. Isotopic patterns in modern global precipitation. In: Swart, P.K., Lohman, K.C., McKenzie, J., Savin, S. (Eds.), Climate Change in Continental Isotopic Records. AGU, pp. 1–36.
Rupper, S., Steig, E.J., Roe, G., 2004. The relationship between snow accumulation at Mt. Logan, Yukon, Canada, and climate variability in the North Pacific. J. Clim. 17, 4724–4739.
Salathé Jr, E.P., 2006. Influences of a shift in North Pacific storm tracks on western North American precipitation under global warming. Geophys. Res. Lett. 33, L19820. http://dx.doi.org/10.1029/2006GL026882.
Schmidt, G.A., Hoffman, G., Shindell, D.T., Hu, Y., 2005. Modeling atmospheric stable isotopes and the potential for constraining cloud processes and stratosphere-troposphere water exchange. J. Geophys. Res. 110. http://dx.doi.org/10.1029/2005JD005790.
Schneider, N., Cornuelle, B.D., 2005. The forcing of the Pacific Decadal Oscillation. J. Clim. 18, 4355–4373.
Seager, R., Ting, M., Held, I., Kushnir, Y., Lu, J., Vecchi, G., Huang, H., Harnik, N., Leetmaa, A., Lau, N., Li, C., Velez, J., Niak, N., 2007. Model projections of an imminent transition to a more arid climate in southwestern North America. Science 316, 1181–1184.
Shapley, M.D., Ito, E., Donovan, J.J., 2008. Isotopic evolution and climate paleorecords: modeling boundary effects in groundwater-dominated lakes. J. Paleolimnol. 39, 17–33.
Shapley, M.D., Ito, E., Donovan, J.J., 2009. Lateglacial and Holocene hydroclimate inferred from a groundwater flow-through lake, Northern Rocky Mountains, U.S.A. The Holocene 19, 523–535.
Shinker, J.J., Bartlein, P.J., 2009. Visualizing the large-scale patterns of ENSO-related climate anomalies in North America. Earth Interact. 13, 3. http://dx.doi.org/10.1175/2008EI2114.1.
Steinhilber, F., Abreu, J.A., Beer, J., Brunner, I., Christi, M., Fischer, H., Heikkilä, U., Kubik, P.W., Mann, M., McCracken, K.G., Miller, H., Miyahara, H., Oerter, H., Wilhems, F., 2012. 9,400 years of cosmic radiation and solar activity from ice cores and tree rings. Proc. Natl. Acad. Sci. 109, 5967–5971.
Steinman, B., Abbott, M.B., 2013. Isotopic and hydrologic responses of small closed lakes to climate variability: hydroclimate reconstructions from lake sediment oxygen isotope records and mass balance models. Geochim. Cosmochim. Acta 105, 342–359.
Steinman, B., Rosenmeier, M.F., Abbott, M.B., 2010. The isotopic and hydrologic response of small, closed-basin lakes to climate forcing from predictive models: simulations of stochastic and mean-state precipitation responses. Limnol. Oceanogr. 55, 2246–2261. http://dx.doi.org/10.4319/lo.2010.55.6.2246.
Steinman, B., Abbott, M.B., Mann, M.E., Stansell, N.D., Finney, B.P., 2012. 1,500 year quantitative reconstruction of winter precipitation in the Pacific Northwest. Proc. Natl. Acad. Sci. 109. http://dx.doi.org/10.1073/pnas.1201083109.
Steinman, B., Abbott, M.B., Mann, M.E., Ortiz, J.D., Feng, S., Pompeani, D.P., Stansell, N.D., Anderson, L., Finney, B.P., Bird, B.W., 2014. Ocean–atmosphere forcing of centennial hydroclimate variability in the Pacific Northwest. Geophys. Res. Lett. 41. http://dx.doi.org/10.1002/2014GL059499.
Steinman, B.A., Abbott, M.B., Nelson, D.B., Stansell, N.D., Finney, B.P., Bain, D.J., Rosenmeier, M.F., 2013. Isotopic and hydrologic responses of small, closed lakes to climate variability: comparison of measured and modeled lake level and sediment core oxygen isotope records. Geochim. Cosmochim. Ac. 105, 455–471.
Stevens, L.R., Stone, J.R., Campbell, J., Fritz, S.C., 2006. A 220-yr record of hydrologic variability from Foy Lake, Montana, USA, inferred from diatom and geochemical data. Quat. Res. 65, 264–274.
Sun, D., 2010. The diabatic and non-linear aspects of the El Niño-Southern Oscillation: implications for its past and future behavior. In: Sun, D. (Ed.), Climate Dynamics: Why Does Climate Vary. American Geophysical Union, Washington DC.
Trenberth, K.E., Hurrell, J.W., 1994. Decadal atmosphere–ocean variations in the Pacific. Clim. Dyn. 9, 303–319.

Wake, C.P., Yalcin, K., Gundestrup, N.S., 2003. The climate signal recorded in the oxygen-isotope, accumulation and major-ion time series from the Eclipse ice core, Yukon Territory. Canada. Ann. Glaciol. 35, 416–422.
Whitlock, C., Dean, W.E., Fritz, S.C., Stevens, L.R., Stone, J.R., Power, M.J., Rosenbaum, J., Pierce, K.L., Bracht-Flyr, B., 2013. Holocene seasonal variability inferred from multiple proxy records from Crevice Lake, Yellowstone National Park, U.S.A. Palaeogeogr. Palaeoclimatol. Palaeoecol. 331–332, 90–103.
Winnick, M.J., Chamberlain, C.P., Caves, J.K., Welker, J.M., 2014. Quantifying the isotopic 'continental effect'. Earth Planet. Sci. Lett. 406, 123–133.
Wise, E.K., 2010. Spatiotemporal variability of the precipitation dipole transition zone in the western United States. Geophys. Res. Lett. 37, L07706. http://dx.doi.org/10.1029/2009GL042193.
Wise, E., 2012. Hydroclimatology of the U.S. Mountain West. Prog. Phys. Geogr. 36, 458–479.
Woodruff, J.D., Donnelly, J.P., Okusu, A., 2009. Exploring typhoon variability over the mid-to-late Holocene: evidence of extreme coastal flooding from Kamikoshiki, Japan. Quat. Sci. Rev. 28, 1774–1785.
Yuan, F., Linsley, B.K., Lund, S.P., McGeehin, J.P., 2004. A 1200 year record of hydrologic variability in the Sierra Nevada from sediments in Walker Lake, Nevada. Geochem. Geophys. Geosyst. 5, Q03007. http://dx.doi.org/10.01029/02003GC000652.
Yuan, F., M.R., K., Valdez, A., 2013. Late glacial and Holocene records of climatic change in the southern Rocky Mountains from sediments in San Luis Lakes, Colorado, USA. Palaeogeogr. Palaeoclimatol. Palaeoecol. 392, 146–160.